Decorin role in extracellular vesicles used to prevent post-operative atrial fibrillation

Simran Rakhra

Thesis submitted to the University of Ottawa
in partial Fulfillment of the requirements for the
Master of Science in Cellular & Molecular Medicine

Department of Cellular and Molecular Medicine
Faculty of Medicine
University of Ottawa

Table of Contents

Acknowledgements

Thesis Advisory Committee

I would like to express my gratitude to my Thesis Advisory Committee members, Dr. Han Kim and Dr. Wenbin Liang. Their guidance and thorough feedback helped me grow as a researcher and successfully complete my thesis. Their expertise allowed me to develop stronger molecular biology and critical thinking skills to refine my work.

Research Team and Collaborators

I am grateful to the members of the Cardiac Translational Research Laboratory: PI Dr. Darryl R. Davis, Dr. Noreen Ahmed, and Dr. Kamal Malhotra. I also wish to thank my colleagues for their support and for creating such a stimulating research environment. Their collective support and expertise were critical to the success of this project.

Technical and Facility Support

I would like to acknowledge the technical expertise provided by the SickKids Cellular and Molecular Electron Microscopy (CMEM) Facility. I extend a special thanks to Dr. Ali Darbandi for providing essential technical assistance that was critical for processing my TEM samples.

I would also like to acknowledge the expertise and training provided by University of Ottawa Heart Institute Flow Cytometry Facility. A special thanks to Dr. Bin Ye for providing training and support that was essential for me to characterize my primary human cells. Their support was invaluable for this project.

Family and Friends

Finally, I want to thank my family and friends for their encouragement and support throughout my graduate studies. Their belief in my abilities was a constant source of motivation, providing me with the resilience to persevere through experimental failures and challenges. I am grateful for their unconditional help and understanding, even though they may not have fully understood the scientific complexities of my work. This achievement is a testament to their continuous encouragement

Abstract

Postoperative atrial fibrillation (AF) affects one-third of patients following cardiac surgery, increasing the risk of stroke. Inflammation-driven atrial fibrosis contributes to postoperative AF. Our lab is investigating the use of extracellular vesicles (EVs) derived from human atrial explant cells to mitigate atrial fibrosis and prevent AF. While EVs have demonstrated protective effects, the underlying mechanisms remain incompletely understood. Recently, our proteomic analysis revealed that EVs are enriched in decorin, an extracellular matrix protein known for its antifibrotic properties. This study investigates whether decorin helps EVs reduce atrial fibrosis by inhibiting profibrotic pathways. This investigation involves a comparison between EVs that contain decorin and those depleted of it. My findings confirm that decorin is highly enriched in EVs and demonstrate that decorin treatment reduces fibroblast proliferation stimulated by TGF-β1. Additionally, DsiRNA knockdown depletes decorin from EVs, providing a model to assess its role. Decorin-enriched EVs significantly reduced cell proliferation compared to decorin-depleted EVs. This suggests that decorin plays a significant role in addition to other factors contributing to the antifibrotic effect of EVs.

List of Tables

List of Figures

Figure 4. Hoechst images of human atrial fibroblasts. Fibroblasts were seeded at varying densities including 1000, 2000, 3000, and 4000 cells in a 96 well plate. Cells were treated with **(A)** 0 ng/mL of TGF-β1 (n=1 technical replicate, n=1 biological replicate), **(B)** 5 ng/mL of TGF-β1 (n=1 technical replicate, n=1 biological replicate), **(C)** 10 ng/mL of TGF- β1 (n=1 technical replicate, n=1 biological replicate) for 48 hours. Fluorescent microscopy was used to capture images at 5x magnification that show the Hoechst-stained nuclei of the cells. The scale bar represents 100 μm.

Figure 5. Isolation of Extracellular Vesicles from human explant derived cells (EDC). (A) Schematic overview of the extracellular vesicle isolation from EDCs conditioned media. **(B)** The Nanoparticle Tracking Analysis (NTA) instrument determines the concentration of the isolated EVs and displays the particle sizes within this sample **(C)** This image represents a single frame from a 60-second NTA video acquisition using the sample presented in (B). Individual extracellular vesicles (EVs) are visible as bright points of scattered light, exhibiting Brownian motion within the sample volume. The software tracks the movement of these particles to determine their diameter and concentration. **(D)** NTA of a second extracellular vesicle sample shows particle concentration and size distribution. **(E)** NTA of a third EV sample's concentration and size distribution was measured. n=3 biological replicates, and n=1 technical replicate.

Figure 6. Transmission electron microscopy (TEM) imaging of extracellular vesicles. A transmission electron microscope was used to take images of a fixed extracellular vesicles sample at the following magnifications: **(A)** 20,000 x (scale bar: 200 nm) **(B)** 25,000 x (scale bar: 200 nm) **(C)** 30,000 x (scale bar: 200 nm) **(D)** 60,000 x (scale bar: 100 nm) **(E)** 80,000 x (scale bar: 100 nm) **(F)** 100,000 x (scale bar: 50 nm). The yellow arrows were used to highlight extracellular vesicles within the above panels. The scale bars for each image is located in the bottom right corner. n=6 technical replicates, and n=1 biological replicate.

Figure 7. Transmission electron microscopy (TEM) imaging used to localize decorin within extracellular vesicles. To localize decorin images were taken at the following magnifications: **(A)**

50,000x magnification (scale bar: 100 nm) **(B)** 150,000x magnification (scale bar: 50 nm) **(C)** 150,000x magnification (scale bar: 50 nm) Yellow arrows highlight extracellular vesicles within these images, and orange arrows highlight decorin within these panels. n=2 biological replicates, and n=1-2 technical replicates per biological replicate.

Figure 8. qPCR confirmation of decorin knockdown. Quantitative polymerase chain reaction (qPCR) was conducted on human explant-derived cells (EDC) cell lysate (n=2 technical replicates, n=1 biological replicate). Human atrial fibroblasts seeded in a 6-well plate were treated with siRNA and control mimic for 24 hours. siRNA and control mimic treatment were facilitated using lipofectamine 2000 reagent. Values are shown as mean ± standard deviation (1 DsiRNA: 1.5 ± 1.7 and Control Mimic: 1.4 ± 1.4). Unpaired t-test was used to determine statistical difference between these groups ($p \leq 0.05$). **Figure 9. qPCR and ELISA confirmation of decorin knockdown.** Human atrial fibroblasts were seeded in a 12-well plate and treated with 2 siRNA (20 nM each) and control mimic. The siRNA and control mimic treatment were facilitated using lipofectamine RNAiMAX reagent. **(A)** The cell lysate was obtained and used to conduct qPCR(n=2 technical replicates, n=1 biological replicate). Values are shown as mean ± standard deviation (2 DsiRNA: 0.99 ± 0.48 and Control Mimic: 1.25 ± 1.07). Unpaired t-test was used to determine statistical difference ($p \leq 0.05$) .**(B)** EDC conditioned media was used to conduct ELISA to confirm protein level knockdown (n=2 technical replicates, n=1 biological replicate). Values are shown as mean ± standard deviation (2 DsiRNA: 253 ± 21.4 and Control Mimic: 687 ± 88). Unpaired test was used to determine statistical difference ($p \leq 0.05$).

Figure 10. EDCs decorin knockdown using siRNA in a 24-well plate. These cells were seeded in a 24well plate and exposed to two treatments: control mimic, and decorin siRNA. **(A)** After 72 hours, qPCR was used to evaluate gene expression using cell lysate (n=4 technical replicates, n=1 biological replicate). Values are shown as mean ± standard deviation (3 DsiRNA: 0.025 ± 0.015 and Control Mimic: 1.04 ± 0.33). Unpaired t-test was used to determine statistical difference ($p \leq 0.05$). **(B)** After 72 hours, ELISA

was used to determine decorin's concentration within EDCs conditioned media (n=3 technical replicates, n=1 biological replicate). Values are shown as mean ± standard deviation (3 DsiRNA:111.76 ± 6.55 and Control Mimic: 4389.69 ± 364.61). Unpaired t-test was used to determine statistical difference ($p \leq 0.05$).

Figure 11. EDCs EVs depletion of decorin using siRNA in petri dishes. These cells were seeded in petri dishes and exposed to three treatments: vehicle, control mimic, and dsiRNA. After 72 hours, the EDCs conditioned media were processed to obtain extracellular vesicles (EVs), and the cell lysate was obtained. **(A)** After 72 hours, qPCR was used to evaluate gene expression using cell lysate (n=3 technical replicates, n=1 biological replicate). Values are shown as mean ± standard deviation (Vehicle: 1.01 ± 0.2, Control Mimic: 2.03 ± 0.9, and 3 DsiRNA: 0.0097 ± 0.007). One-way ANOVA with Tukey's post hoc test. **(B)** After 72 hours, ELISA was used to determine decorin's concentration within EDCs EVs (n=3 technical replicates, n=1 biological replicate). Values are shown as mean ± standard deviation (Vehicle: 344 ± 38, Control Mimic: 323 ± 12.56, and 3 DsiRNA: 8.96 ± 5.29). One-way ANOVA with Tukey's post hoc test.

Figure 12. DCN has no effect on cell proliferation. Human atrial fibroblasts were seeded in 96-well plates. After 24 hours of seeding, these cells were treated with 1 μg/mL DCN, 10 μg/mL DCN, and TGFβ1 (10 ng/mL). **(A)** After 48 hours of treatment, cells proliferation was assessed using cell counting kit-8 (CCK-8)(n=3 technical replicates, n=1 biological replicate). This dye is added to the wells consisting of cells and incubated. The optical densities are measured using a microplate reader. Values are shown as mean ± standard deviation (Control: 0.78 ± 0.05, 1 μg/mL DCN: 0.79 ± 0.04 ,10 μg/mL DCN: 0.743 ± 0.04, TGF-β1: 1.04 ± 0.07). One-way ANOVA with Tukey's post hoc test. Significant differences are shown as $p \leq 0.05$. **(B)** After 24 hours of treatment, cell proliferation was assessed using Hoechst staining (n=3-4 technical replicates, n=1 biological replicate). The stained nuclei within the wells are imaged using a fluorescent microscope at 365 nm filter. The nuclei were counted using ImageJ. Values are shown as mean ± standard deviation (Control:1999.5 ± 151.5, 1 μg/mL DCN: 2144.875 ± 182. 9,10

µg/mL DCN: 2364.58 ± 127.2, TGF-β1: 2758.16 ± 312.6). One-way ANOVA with Tukey's post hoc test. Significant differences are shown as $p \leq 0.05$.

Figure 13. Hoechst-stained images of a well seeded human atrial fibroblasts separately treated with DCN and TGF-β1. Human atrial fibroblasts were seeded in a 96-well plate. After 24 hours, these cells were treated separately with (A) media (n=1 technical replicate, n=1 biological replicate) (B) TGF-β1 (10 Page 10 of 68 ng/mL) (n=1 technical replicate, n=1 biological replicate) (C) 1 µg/mL DCN (n=1 technical replicate, n=1 biological replicate) (D) 10 µg/mL DCN (n=1 technical replicate, n=1 biological replicate). After 24 hours of treatment, wells were treated with Hoechst to stain nuclei. Four images of each well were captured using a fluorescent microscope at a 5 x magnification. In this figure, one well with each treatment was illustrated but the other wells are shown in the supplementary figures. The nuclei were counted using ImageJ. The scale bar represents 100 µm.

Figure 14. DCN inhibits TGF-β1 proliferative activity. Human atrial fibroblasts were seeded in 96well plates. 24 hours later, these cells were treated with 1 µg/mL DCN and 10 µg/mL DCN. After 24 hours of decorin treatment, these cells were treated with TGF-β1 (10 ng/mL). **(A)** After 48 hours of treatment, cell proliferation was assessed using cell counting kit-8 (CCK-8) (n=3-4 technical replicates, n=1 biological replicate). The optical density was measured at 450 nm using a microplate reader. Values are shown as mean ± standard deviation (Control: 0.73 ± 0.02, 1 µg/mL DCN + TGF-β1: 0.76 ± 0.05,10 µg/mL DCN + TGF-β1: 0.73 ± 0.02, TGF-β1: 0.89 ± 0.04). One-way ANOVA with Tukey's post hoc test. Significant differences are shown as $p \leq 0.05$. **(B)** After 24 hours of treatment, cell proliferation was measured using Hoechst staining (n=4 technical replicates, n=1 biological replicate). The wells containing the cells where imaged using a fluorescent microscope at a 365 nm filter. The nuclei were counted using ImageJ. Values are shown as mean ± standard deviation (Control: 3521 ± 302.5, 1 µg/mL DCN + TGFβ1: 3209.8 ± 321.67, 10 µg/mL DCN + TGF-β1: 3402.56 ± 159.58, TGF-β1: 4360.375 ± 105.4). One-way ANOVA with Tukey's post hoc test. Significant differences are shown as $p \leq 0.05$.

Figure 15. Hoechst-stained images of human atrial fibroblasts co-treated with DCN (1 µg/mL or 10 µg/mL) and TGF-β1 (10 ng/mL). Cells are seeded on 96-well plates. These cells are treated with **(A)** media (n=1 technical replicate, n=1 biological replicate) **(B)** TGF-β1 (n=1 technical replicate, n=1 biological replicate) **(C)** 1 µg/mL decorin with TGF-β1(n=1 technical replicate, n=1 biological replicate) **(D)** 10 µg/mL decorin with TGF-β1 (n=1 technical replicate, n=1 biological replicate). 24-hour post-treatment, wells were treated with Hoechst to stain the nuclei. The wells were imaged using a fluorescent microscope and nuclei were counted using ImageJ. In this figure, one well per treatment is displayed, and the remaining wells are shown in the supplementary figures. The scale bar represents 100 µm. **Figure 16**. **NanoSight Tracking Analysis of decorin-enriched and decorin-depleted EVs. (A)** This image represents a single frame from a 60-second NTA video acquisition of the DsiRNA EV sample. **(B)** This image represents a single frame from a 60-second NTA video acquisition of the control mimic EV sample. n=1 biological replicate, and n=1 technical replicate. **(C)** This histogram represents the NanoSight data for the DsiRNA EV sample. n=1 biological replicate, and n=1 technical replicate. **(D)** This histogram represents the nanosight data for the Control Mimic EV sample.

Figure 17. EVs depleted of decorin do not prevent TGF-β1 induced cell proliferation. Human atrial fibroblasts were seeded in 96-well plates. After 24 hours of seeding, cells were treated with decorin enriched and decorin-depleted EVs. A ratio of 10,000 EVs per human atrial fibroblast was used to normalize decorin-enriched and depleted EVs. After 24 hours, EV treated cells were exposed to TGF-β1 treatment. **(A)** After 48 hours of treatment, CCK-8 reagent was added into each well. The optical density of these wells was measured at 450 nm (n=3-4 technical replicates, n=1 biological replicate). Values are shown as mean ± standard deviation (Control: 1.62 ± 0.04, EVs (Control Mimic): 1.67 ± 0.04, EVs (DsiRNA) + TGF-β1: 1.75 ± 0.02, TGF-β1: 1.8305 ± 0.05). One-way ANOVA with Tukey's post hoc test. Significant differences are shown as $p \leq 0.05$. **(B)** After 24 hours of treatment, Hoechst staining was used to stain cells nuclei (n=3-4 technical replicates, n=1 biological replicate). These cells were imaged using a

fluorescent microscope at 365 nm filter. The nuclei were counted using ImageJ. Values are shown as mean ± standard deviation (Control: 87.875 ± 3.12, EVs (Control Mimic): 77.875 ± 9.33, EVs (DsiRNA) + TGF-β1: 108.375 ± 2.62, TGF-β1: 106 ± 9.85). One-way ANOVA with Tukey's post hoc test. Significant differences are shown as $p \leq 0.05$.

Figure 18. Hoechst-stained images of human atrial fibroblasts co-treated with extracellular vesicles and TGF-β1. Human atrial fibroblasts were seeded in 96-well plates. These cells were treated with **(A)** media (n=1 technical replicate, n=1 biological replicate) **(B)** TGF-β1 (n=1 technical replicate, n=1 biological replicate) **(C)** EVs (control mimic) with TGF-β1 (n=1 technical replicate, n=1 biological replicate), and **(D)** EVs (DsiRNA) with TGF-β1(n=1 technical replicate, n=1 biological replicate). 24 hours later, Hoechst was added into each well to stain the nuclei. The nuclei were imaged using a fluorescent microscope. The scale bar represents 100 μm.

Supplementary Figure S1. Hoechst images of human atrial fibroblasts. Fibroblasts were seeded at varying densities including **(A)** 1000, **(B)** 2000, **(C)** 3000, and **(D)** 4000 cells in a 96 well plate. Cells were treated with 0 ng/mL of TGF-β1, 5 ng/mL of TGF-β1, 10 ng/mL of TGF- β1 for 48 hours. Fluorescent microscopy was used to capture images at 5x magnification that show the Hoechst-stained nuclei of the cells in the wells. The scale bar represents 100 μm. n=2 technical replicates per condition. These cells were from one biological sample (n=1 biological replicate).

Supplementary Figure S2. Hoechst-stained images of a wells seeded human atrial fibroblasts separately treated with DCN and TGF-β1. Human atrial fibroblasts were seeded in a 96-well plate. After 24 hours, these cells were treated separately with **(A)** media (n=3 technical replicates) **(B)** TGF-β1 (10 ng/mL) (n=3 technical replicates) **(C)** 1 μg/mL DCN (n=3 technical replicates) **(D)** 10 μg/mL DCN (n=2 technical replicates). These cells were from one biological sample (n=1 biological replicate). After 24 hours of treatment, wells were treated with Hoechst to stain nuclei. Four images of each well were captured using a fluorescent microscope at a 5 x magnification. The nuclei were counted using ImageJ. The scale bar represents 100 μm.

Supplementary Figure S3. Hoechst-stained images of human atrial fibroblasts co-treated with DCN (1 µg/mL or 10 µg/mL) and TGF-β1 (10 ng/mL). Cells are seeded on 96-well plates. These cells are treated with **(A)** media **(B)** TGF-β1 **(C)** 1 µg/mL decorin + TGF-β1 **(D)** 10 µg/mL decorin + TGF-β1. 24-hour post- treatment, wells were treated with Hoechst to stain the nuclei. The wells were imaged using a fluorescent microscope and nuclei were counted using ImageJ. The scale bar represents 100 µm. n=3 technical replicates per condition. These cells were from one biological sample (n=1 biological replicate).

Supplementary Figure S4. Hoechst-stained images of human atrial fibroblasts co-treated with extracellular vesicles and TGF-β1. Human atrial fibroblasts were seeded in 96-well plates. These cells were treated with **(A)** media **(B)** TGF-β1 **(C)** EVs (control mimic) with TGF-β1, and **(D)** EVs (DsiRNA) with TGF-β1. 24 hours later, Hoechst was added into each well to stain the nuclei. The nuclei were imaged using a fluorescent microscope. The scale bar represents 100 µm. n=3 technical replicates per condition. These cells were from one biological sample (n=1 biological replicate).

List of Symbols, Abbreviations or Nomenclature

AF	Atrial fibrillation
ANOVA	Analysis of variance
CCK-8	Cell Counting Kit-8
DCN	Decorin
DMEM	Dulbecco's Modified Eagle Medium
DsiRNA	Dicer-substrate small interfering RNA
ECM	Extracellular matrix
EDC	Human explant derived cells
ELISA	Enzyme – linked immunosorbent assay
EV	Extracellular vesicle
FBS	Fetal bovine serum
IHC	Immunohistochemistry
NTA	Nanosight Tracking Analysis
PBS	Phosphate-buffered saline
PFA	Paraformaldehyde
POAF	Post-operative atrial fibrillation
qPCR	Quantitative Polymerase Chain Reaction
RCF	Relative centrifugal force
RPM	Revolutions per minute
SLRP	Small leucine-repeat proteoglycan

TEM	Transmission electron microscope
TGF-β1	Transforming growth factor beta-1
UC	Ultracentrifuge

Introduction

Post-operative atrial fibrillation (POAF) is a common type of atrial fibrillation (AF) experienced by 30% of patients undergoing cardiac surgery.[1] This is an asymptomatic condition that only persists for 2-4 days post-surgery, however it can have detrimental effects on patients.[1] POAF is associated with long hospital stays, stroke, myocardial infarction, heart failure, and mortality.[1] While this condition can also affect patients undergoing non-cardiac (thoracic) surgery, the incidence of POAF among these patients is less than cardiac surgery patients.[1] During cardiac surgery, there are a variety of complications that can arise leading to POAF including injury to atrial myocardium, and inflammation.[1] An injury to the atrial myocardium could cause disruptions in the heart's conduction processes leading to re-entry.[1] A concept where a specific part of the heart is constantly propagated with electrical impulses leading to AF.[2] Furthermore, cardiac surgery can also contribute to POAF by causing the body to have an inflammation response to the surgical injuries. [3] As a result of this, inflammatory markers and cytokines are higher in POAF patients compared to other patients.[3] There have been many efforts to prevent POAF using various medications as this condition can compromise a patient's quality of life.

Beta blockers and amiodarone are medications commonly used in clinical settings to reduce POAF incidence.[4] Beta blockers can be used for a variety of cardiovascular conditions as they exhibit a diverse array of effects including anti-arrhythmic and anti-ischaemic.[5] Despite these benefits, betablockers can also cause a variety of complications like bradycardia, atrioventricular block, and symptomatic hypotension.[5] On the other hand, amiodarone does not exhibit as many benefits as betablockers, and causes complications like QT prolongation, and torsade de pointes.[4] Currently, the POAF prevention strategy involves beta blockers/amiodarone followed by anticoagulants and rhythm control drugs.[4] This strategy illustrates the challenges of preventing POAF as a variety of drugs are involved in this process that also have side effects. Hence, our laboratory (Cardiac Translational Research

Laboratory) generates extracellular vesicles (EVs) that exerts anti-fibrotic effects and reduces inflammation to prevent POAF.

EVs are membrane bound particles that have a diameter of <200 nm and are secreted by various cell types.[6] To classify these particles as EVs, they were characterized using a proteomic array and flow cytometry.[7] It was determined that the particles consist of the following transmembrane and cytosolic markers: CD63, CD81, FLOT1, ICAM1, EpCam, ANXA5, ALIX, and TSG101.[7] CD63 and CD81 are tetraspanin proteins, which are enriched in EVs.[8] FLOT1 is part of the flotillin family which plays a role in internalizing EVs.[9] Intercellular adhesion molecules (ICAM-1)is highly enriched in EVs that are derived from HUVEC cells.[10] Epithelial cell adhesion molecule (EpCAM) is highly expressed in EVs derived from cancer and stem cells.[11] Annexin A5 (ANXA5) binds to PS, which is a lipid phosphatidylserine that is present in animal cell plasma membranes, and the outer surfaces of EVs.[12] Therefore, Annexin A5 can be useful in classifying particles as EVs.[12] Lastly, ALIX and TSG101 are ESCRT accessory proteins that regulate and transport EVs.[8]

In this lab, extracellular vesicles are produced from cardiac explant-derived cells (EDCs).[13] EDCs are CD45- CD105+ cells cultured using patient atrial appendage biopsies which produce EVs into their conditioned media.[13] Therefore, the EDC conditioned media can be further processed to isolate for EVs. Furthermore, these particles consist of a variety of molecules including proteins, mRNA, and noncoding RNAs.[14] These molecules are important as they allow EVs to communicate with surrounding tissues and cells by uptaking them through processes like fusion.[15] To specifically study the molecules within the EVs cargo, our laboratory conducted a proteome analysis. This analysis demonstrated that EVs consist of 28 proteins associated with reducing fibrosis with decorin being the most expressed.[7]

Decorin is an extracellular matrix (ECM) protein that is a member of the small leucine-rich proteoglycan (SLRP) family. This protein is produced by the endoplasmic reticula and Golgi apparatuses of fibroblasts.[1617] Structurally, decorin has a 42 kDa conserved core, a chondroitin-sulfate (CS) or dermatan-sulfate (DS) side chain, and a concave region that facilitates interactions with other proteins.[16,17]

Decorin interacts with ECM proteins by binding the receptors of growth factors and receptor tyrosine kinases to inhibit cell growth.[17]It can also directly interact with ECM proteins, limiting their availability by binding to them and forming complexes.[17] Decorin prevents fibrosis by binding directly to transforming growth factor beta-1 (TGF-β1) and forming a complex,[16] thus reducing its availability and inhibiting fibrotic signaling.[17]

Transforming growth factor β (TGF-β) is a family of cytokines that are produced by somatic human cells.[18] This family consists of three different human isoforms including TGF-β1, β2, and β3.[19] All of these forms are ligands that bind to the following receptors: TβRI, II, III to activate a signaling cascade that can affect processes like cell proliferation, migration, and other processes.[18] To participate in various cell processes, TGF-β needs to be in its active form as it consists of a latency-associated peptide (LAP).[20] This growth factor is activated when LAP is cleaved proteolytically, or when its RGD (arginine-glycineaspartic acid) binds with ITGAV/αv integrins.[19] Integrins, acids, bases, reactive oxygen species (ROS), thrombospondin-1 (TSP-1) and many other factors play a role in activating TGF-β.[20] Once active, TGF-β uses the TβRI and TβRII receptors to activate the SMAD pathway in cells.[20] TGF-β1 and β3 either binds to TβRII homodimer or initializes its homodimerization upon binding.[20] This allows the receptor to recruit TβRI, a receptor that TGF-β1 and β3 bind to with poor affinity.[20] Compared to TGF-β3, TGF-β1 structure has been well characterized.[19] In addition to this, it is also known induce organ fibrosis by transforming fibroblasts into myofibroblasts.[19]

In this study, decorin role in extracellular vesicles was evaluated by modifying EVs to generate EVs enriched with decorin and depleted of decorin. These EVs were tested using an in vitro model of inflammation which was induced by TGF-β1.

Study Rationale, Aims, & Hypothesis

Study Rationale

About a million adults in North America and Europe are undergoing cardiac surgery each year.[21] These patients may be affected by POAF post-surgery, as this condition is associated with increased hospital stay and health issues like infection, and stroke.[22] As a consequence, it causes patients to experience short-term and long-term complications like stroke, infarction, and internal bleeding.[23] In addition to this, it can also increase the risk of mortality within 30 days – 6 months post-surgery.[23] Thus, making it important to have therapeutics that can prevent POAF. Extracellular vesicles (EVs) have been highlighted in clinical research as they are involved in cell-cell communication.[24] During normal and diseased physiological conditions, most eukaryotic cells generate EVs and release them into extracellular matrix.[24] These molecules consist of microRNA (miRNAs), messenger RNAs (mRNAs), proteins, and lipids, which are used to elicit a response in the recipient cell.[24] Recently, our lab has determined that EVs produced by human explant derived cells (EDCs) are capable of preventing post-operative atrial fibrillation.[7] Proteomic analysis of these EVs determined that they are enriched with decorin which may be contributing to their antifibrotic potential.[7] Therefore, this study aims to determine if decorin depletion significantly alters the potential of EVs to prevent POAF.

Aims

The aims of this study are to characterize the effect of decorin knockdown in EDCs on EV formation and composition, establish decorin relationship with TGF-β1 in inhibiting fibroblast proliferation, and to evaluate the impact of decorin knockdown on EVs ability to influence human atrial fibroblasts proliferation.

Hypothesis

Decorin contributes to the ability of extracellular vesicles to reduce atrial fibrosis, thereby aiding in the prevention of atrial fibrillation.

Materials & Methods

Cell Culture

Primary Human Explant-Derived Cells (EDCs)

Human explant-derived cells (EDCs) were obtained from patient atrial appendage biopsies. These cells were grown at 5% O_2 at 37˚C in T75 or T175 flasks containing 20% CEM (78% IMDM, 20% HI F BS, 1% anti-anti, 1% L-Glutamine, 0.18% BME). For long term storage, EDCs were stored in the -80°C freezer.

Primary Human Atrial Fibroblasts

To conduct in vitro experiments, primary human atrial fibroblasts were isolated and cultured. Human atrial appendages were obtained from consenting patients undergoing cardiac surgery in the University of Ottawa Heart Institute (UOHI). The samples were minced and digested using collagenase IV (Gibco, 17104019). To ensure the cells grew well, Dulbecco's Modified Eagle Medium (Gibco, 11965118) was supplemented with 20% FBS (Gibco, A5670701), and 1% anti-anti (Gibco, 15240062). Initially, the cells were placed in a T75 flask to ensure they were in proximity, helping them grow well. However, it was noted that it was difficult to grow cells from older patient atrial appendages. In that case, I decided to place the cells in a T25 flask to ensure they were near each other. Subsequently, the media was changed every 2-3 days to ensure the cells were provided with sufficient nutrition to grow.

Characterize Human Atrial Fibroblasts

I used Flow Cytometry to characterize primary human atrial fibroblasts. First, primary human atrial fibroblasts were isolated and cultured from consenting patients undergoing cardiac surgery at the University of Ottawa Heart Institute (UOHI). Cells were lifted using 3 mL of TrypLE (Gibco,50591420) when they reached 80% confluency within the T175 flasks. After a few minutes of incubation, 6 mL of DPBS (Gibco, 14190144) was added to this solution and resuspended. The cell suspension was centrifuged at 300 RCF for 5 minutes. A cell hemocytometer was used to determine the number of cells within this suspension. 200,000 to 250,000 cells were pipetted into 1.5 mL microcentrifuges. These tubes

were centrifuged at 300 RCF at 4°C for 5 minutes. After centrifugation, the supernatant was disposed and the cell pellet was resuspended with 200 µL of cold DPBS and 5 microliters of CD90, and DDR2 displayed in **Table 1**. The cell suspension containing antibodies was incubated in a 4°C fridge. After 30 minutes of incubation, the cell pellet was washed with cold DPBS twice before processed using the MACSQuant Analyzer 10.

Table 1. List of antibodies used for flow cytometry.

Names	Company	Catalog Number
CD90	BD Biosciences	555596
DDR2 Antibody	Novus Biologicals	FAB25381P

Extracellular vesicle Isolation

30 mL of conditioned media from human explant derived cells (EDCs) were placed into 50 mL falcon tubes. These falcon tubes were placed in -80°C freezer for short-term. The conditioned media was taken out of the -80°C freezer and placed into the 4°C fridge for the media to thaw overnight. After the thawing process, the conditioned media was used for isolation of extracellular vesicles. About 8-9 mL of conditioned media was added into each conical ultracentrifuge tube. Then, these tubes were inserted into the SW41 rotor, and the weight of the tubes were balanced using DPBS to ensure they are within the range of ±0.05g from each tube. The Beckman Coulter Ultra Centrifuge was used to spin the tubes at 8000 RPM, 4°C for 30 minutes. After the spin, the supernatant from these tubes was obtained and placed into new conical ultracentrifuge tubes. These tubes were balanced and spun at 28,000 RPM, 4°C for 3 hours in the Beckman Coulter Ultra Centrifuge. After this spin, the supernatant was disposed carefully to ensure that the pellet wasn't disturbed. The pellets in the three tubes were resuspended using 200 µL of DPBS (Gibco). The resuspended pellets were placed on ice and the Nanosight Tracking Analysis (NTA) instrument was used to determine the concentration of these EVs. These EVs were stored in the -80°C freezer for a short-term. Within this study, EVs were obtained from multiple independent donors. There

was variability between the EV samples concentrations however, the yields were sufficient for downstream assays.

Transmission Electron Microscopy of Extracellular Vesicles

Transmission Electron Microscopy (TEM) was used to localize decorin within extracellular vesicles. To prepare the samples for TEM, petri dishes were incubated with 3 mL of fibronectin for an hour at 37°C. Human explant-derived cells were plated on the fibronectin-coated petri dishes, and incubated at 5% O_2 at 37°C. After 3 days of incubation, the conditioned media from these petri dishes were obtained and processed using ultracentrifugation to obtain extracellular vesicles. The EVs were fixed using 50 µL of 4% paraformaldehyde (PFA). The grids were charged, and the extracellular vesicles sample were placed on the grid and incubated for an hour. After incubation, the grids were washed for 5 minutes using phosphate buffer solution. Permeabilization buffer was diluted to 1X concentration in distilled water, which was applied to the grid for 30 minutes. Then, primary and secondary antibodies provided in **Table 2** were used to stain decorin for about 1-2 hours. 1% glutaraldehyde was used for 10 minutes to fix the sample on the grids. After a wash with 8x distilled water, the grid was incubated with uranyl oxalate for 10 minutes to improve the contrast in the extracellular vesicle images. Lastly, the grid was air dried and used in TEM to obtain images of EVs.

Table 2. Antibodies used for staining Extracellular Vesicles.

Name	Company	Catalog Number
Decorin Monoclonal Antibody (5E8E7)	Invitrogen	FERMA548436
Goat anti-Mouse IgG (H+L) Secondary Antibody, Alexa Fluor™ 488-10 nm colloidal gold	Invitrogen	A31561

Decorin knockdown using small interfering RNA

Small scale knockdown

40,000 EDCs were seeded to 6 wells of the 24-well plate, and media was added to these wells to achieve a total volume of an mL/well. After 24 hours, the wells were transfected using 3 DsiRNA from the

TriFECTa RNAi kit (Integrated DNA Technologies) and lipofectamine RNAiMAX reagent (Invitrogen, 13-778-030). After 72 hours of transfection, the conditioned media, and cell lysate was collected.

Large scale knockdown

A petri dish was coated with 3 mL fibronectin and incubated for 1 hour at 37°C. Subsequently, EDCs from flasks were lifted using TrypLE, centrifuged at 400 RCF for 5 minutes, and manually counted. Following this, 550,000 EDCs were added to each petri dish, and media was added to achieve a total volume of 10 mL/petri dish. After 24 hours, 3 DsiRNA (TriFECTa RNAi kit) with lipofectamine RNAiMAX (Invitrogen, 13-778-030) were used to transfect these petri dishes.-

After 72 hours, the conditioned media and cell lysate was collected to conduct downstream assays.Transcriptional and protein profiling

Small scale

The ability of DsiRNA to knockdown decorin on a transcriptional and protein level was assessed in EDCs. To analyze decorin transcriptional levels, 500 µL of Qiazol lysis reagent was added to the wells containing the cells. Then, the miRNeasy Micro kit (50) was used to perform RNA isolation. The concentration, 260/280 ratio, 260/230 ratio of the isolated RNA was analyzed using a NanoDrop Spectrophotometer. The isolated RNA was used in the quantitative reverse transcription polymerase chain reaction (RT-qPCR) assay by adding 2 µL of iscript (RTase), 200 ng of RNA sample, and filling up the remaining volume with nuclease-free water in PCR tubes. These tubes were placed into a thermocycler with the following conditions: 5 minutes at 25˚C, 20 minutes at 46˚C, and 1 minute at 95˚C. A master mix for the 18S housekeeping gene and the decorin gene is prepared for the qPCR reaction. 6 µL of master mix was added per well with 4 µL of cDNA from RT reactions.

Then, decorin concentration was confirmed using an enzyme linked immune assay (ELISA) kit (Invitrogen, EHDCN). The EDC conditioned media was collected from each well and used in ELISA to confirm knockdown of decorin.

Large scale

DsiRNA knockdown of decorin was evaluated by analyzing gene expression and protein concentration. To analyze changes in gene expression, 700 µL of Qiazol lysis reagent was added to each petri dish. Then, the miRNeasy Micro kit (50) was used to perform RNA isolation. After conducting RNA isolation, a NanoDrop Spectrophotometer was used to analyze the concentration, 260/280 ratio, 260/230 ratio of the isolated RNA. Reverse transcription was used to convert RNA to cDNA. Then qPCR was conducted using master mix for 18S housekeeping and decorin gene, cDNA, and SYBR green.

To analyze changes in protein concentration, EDC conditioned media was collected from the petri dishes. An enzyme linked immune assay (ELISA) (Invitrogen, EHDCN), was used to quantify the protein within EVs.

Functional effects of decorin (in vitro)

Human atrial fibroblasts are grown in Dulbecco's Modified Eagle High Glucose Medium (Gibco, 11965118) and human atrial fibroblasts were seeded in a 96-well plate. After 24 hours, cells were treated with 1, and 10 µg/mL of Decorin from bovine articular cartilage (D8428, Sigma Aldrich). After 48 hours of seeding, wells containing decorin were treated with 10 ng/mL of TGF-β1 (catalogue: GF 346, Millipore Sigma). After 72 hours of seeding, the wells were stained with PureBlu Hoechst 33342 Nuclear Staining Dye (135-1304, BioRad). Then, these wells were imaged using a fluorescent microscope and a 365 nm filter. After 96 hours of seeding, another 96-well plate was treated with 10 µL of Dojindo Molecular Cell Counting Kit-8 (NC0314243, Fisher Scientific). The optical density was measured using a microplate reader.

Functional effects of extracellular vesicles (in vitro)

To test the effects of extracellular vesicles, human atrial fibroblasts were seeded in a 96-well plate. After 24 hours, these cells were treated with decorin-depleted extracellular vesicles (10,000 EVs/human atrial fibroblast) whereas other cells were treated with decorin-enriched extracellular vesicles

(10,000 EVs/human atrial fibroblast). The decorin-depleted and decorin-enriched EV dosage was normalized by particle number. After 48 hours, wells containing decorin-depleted and decorin-enriched EVs were treated with 10 ng/mL of TGF-β1 (catalogue: GF 346,

Millipore Sigma). After 72 hours of seeding, proliferation was analyzed by staining these wells with PureBlu Hoechst 33342 Nuclear Staining Dye (135-1304, Biorad). Then, proliferation was analyzed within a separate 96-well plate using Dojindo Molecular Cell Counting Kit-8 (NC0314243, Fisher Scientific).

Statistical Analysis

Microplates were used for the experiments conducted in this study. For each experimental condition, cells were seeded in multiple wells per plate to reduce variability. The values of wells corresponding to a particular condition were presented as averages (mean ± standard deviation). In addition to this, data within each figure was presented as mean ± standard deviation. The statistical test and the n for each sample were mentioned within the figure legends. Unpaired t-tests were used to analyze statistical differences between two groups. To test the statistical difference between more than two groups, the one-way ANOVA test with Tukey's post hoc test was used. For the initial proliferation assays, two-way ANOVA with Tukey's post hoc test was used. For all figures, variances were assumed to be equal, and normality was confirmed using the Shapiro-Wilk test. A value of $p \leq 0.05$ was considered significant for all statistical tests.

Results

Characterization of Primary Human Atrial Fibroblasts

An in vitro model was established by isolating and culturing primary human atrial fibroblasts (**Figure 1**). To characterize primary human atrial fibroblasts, flow cytometry was used to assess the expressions of fibroblast markers, DDR2, and CD90.[25] **Figure 2A** illustrated a significant increase in CD90 (94-fold increase, $p < 0.05$) and DDR2 (92-fold increase, $p < 0.05$) expression compared to the unstained cells. **Figures 2B and 2C** qualitatively depict these trends in both biological replicates. A right shift is observed from unstained cells (red) to CD90-stained cells (purple) and DDR2-stained cells (blue) in terms of fluorescent intensity. Interestingly, the population of cells within **Figure 2B** has a smaller human atrial fibroblast diameter (nm) compared to cells in **Figure 2C.** In addition to this, **Figure 2B** unstained control cells have a higher fluorescent intensity compared to **Figure 2C** unstained cells. Altogether, this data suggests that these cultured cells are human atrial fibroblasts, and consist of cells with diverse sizes.

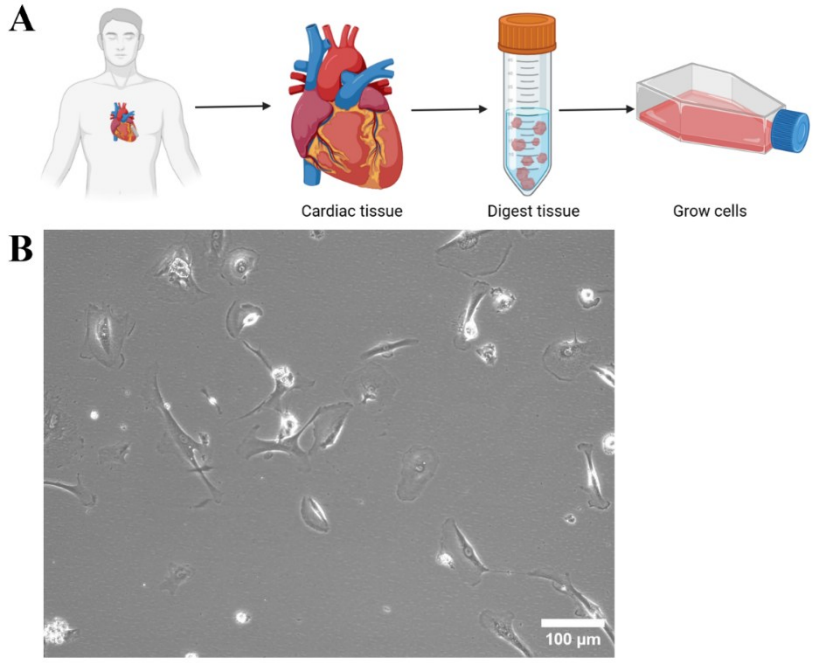

Figure 1. Isolation and culture of human atrial fibroblasts. (A) Schematic of the procedure used to isolate fibroblasts from atrial appendage tissue obtained from consented patients. Tissue was digested

using collagenase IV and plated in flasks. **(B)** Representative fluorescent microscope image of primary human atrial fibroblasts at passage 1 (10x magnification) from one patient (n=1 biological replicate). Scale bar represents 100 µm.

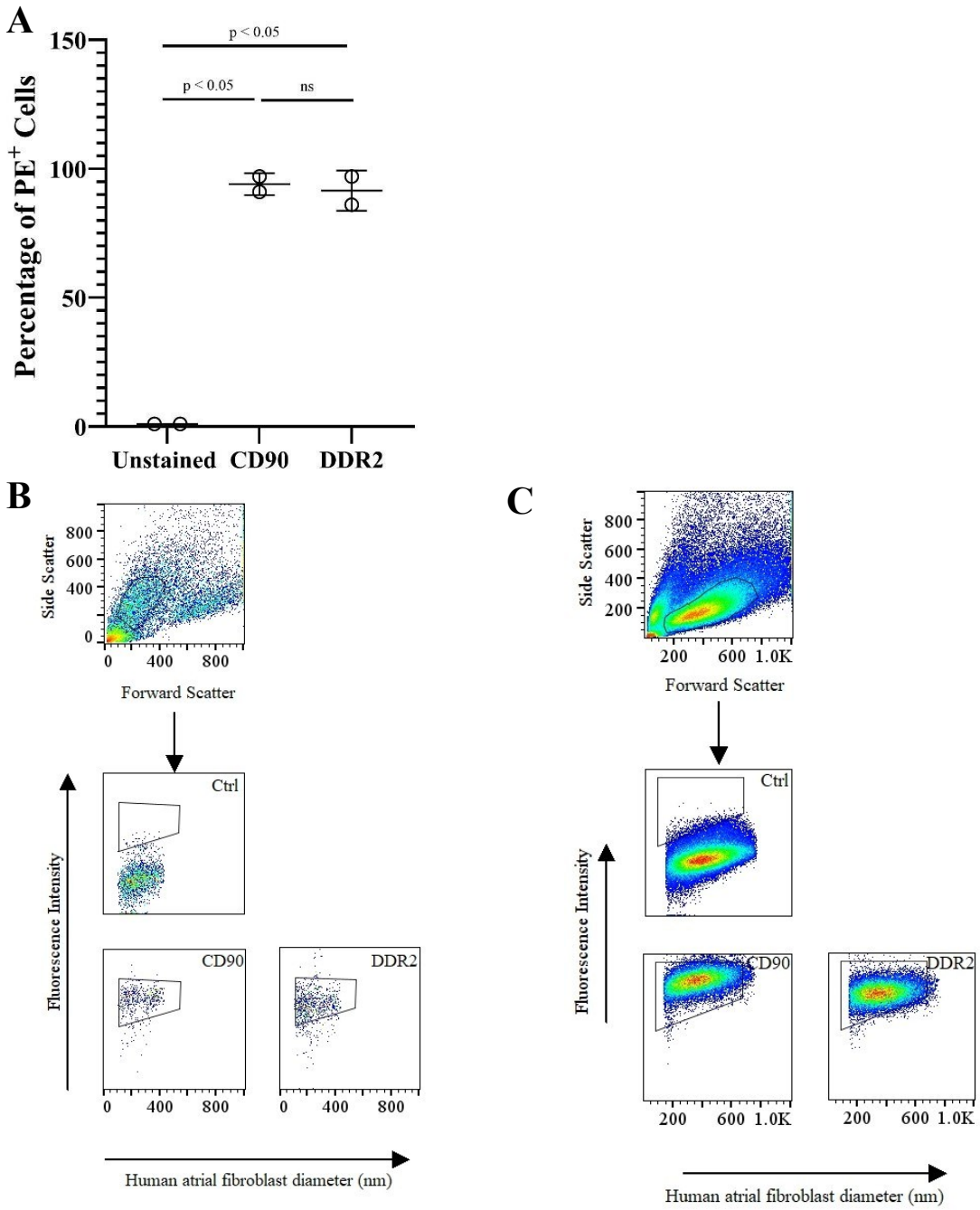

Figure 2. Characterization of primary human atrial fibroblasts. (A) Human atrial fibroblast marker expressions were quantified by calculating the percentage of PE^+ cells in unstained, CD90-stained, and

DDR2-stained cell populations (n = 2 biological replicates, n =1 technical replicate). Values are shown as mean ± SD (Unstained: 1 ± 0; CD90: 94 ± 4.2; DDR2: 91.5 ± 7.8). One-way ANOVA with Tukey's post-hoc test. Significant difference between Unstained and CD90-stained, and Unstained and DDR2-stained ($p \leq 0.05$). **(B)** Representative flow cytometry plots display the gating of the control cell populations (top panel) and the bottom panel illustrate plots of control, CD90-stained, and DDR2 stained cells. **(C)** These are flow cytometry plots of an additional biological replicate which displays gating of control cells (top panel) and stained cells (bottom panel).

TGF-β1 induces proliferation in primary human atrial fibroblasts

To test the anti-fibrotic properties of decorin, and extracellular vesicles in preventing postoperative atrial fibrillation (POAF), TGF- β1 concentrations were optimized in vitro.[26] These concentrations were adjusted to mimic fibrosis which contributes to POAF.[27] To induce fibroblast proliferation, 5 and 10 ng/mL of TGF-β1 was delivered to wells containing 1000, 2000, 3000, 4000, and 5000 cells (**Figure 3**). Subsequently, cell proliferation was assessed using CCK-8 and Hoechst-staining. CCK-8 was used to determine the optical density of wells at 450 nm (**Figure 3A**). In addition to this, Hoechst was used to determine the average number of cells per the fluorescent microscope's field of view at 5x magnification (**Figure 3B**).

Post-48 hours of cell treatment with TGF-β1 (5, and 10 ng/mL), the wells were treated with CCK8(**Figure 3A**). This method illustrates the relationship between cell densities per well and the absorbance of the formazan dye measured in optical density (O.D.). The trend seen between these variables reveals a positive correlation since as the cell densities per well increase, the O.D. values increase. A comparison between the control wells consisting of 1000 and 2000 cells per well, revealed ~1.4-fold increase in the O.D. values. Interestingly, ~1.1 fold-decrease was observed in the O.D. values of 3000 cells/well to 4000 cells/well. From 4000 cells/well to 5000 cells/well, there was ~1.23 fold-increase observed in O.D. values. When TGF-β1 was administered to wells containing 1000, 2000, and 3000 cells,

no significant differences were observed in O.D. compared to control ($p > 0.05$, **Figure 3A**). However, 4000 cells/well treated with 5 ng/mL of TGF-β1 had a 1.23-fold increase in O.D. compared to control ($p < 0.05$, **Figure 3A**). A similar fold-increase was seen when 4000 cells/well were treated with 10 ng/mL of TGF-β1. This resulted in an optical density increase of 1.2-fold compared to control ($p < 0.05$, **Figure 3A**). For 5000 cells per well, there was only a significant difference between the cells with no treatment and cells receiving 10 ng/mL of TGF-β1 (1.24-fold increase, $p < 0.05$, **Figure 3A**).

To corroborate the findings from the CCK-8 assay, Hoechst was used to stain the nuclei of primary human atrial fibroblasts seeded in a 96-well plate. As the number of cells increased in each control well, the average number of cells/field of view increased, which was observed in the images taken using a fluorescent microscope (**Figure 4, Supplementary Figure S1**). However, TGF-β1 administration produced differing trends across the cell densities. At 1000 cells/well, there was no significant difference seen between the control wells and those treated with 5 ng/mL and 10 ng/mL of TGF- β1 ($p> 0.05$, **Figure 3B**). As the cell density increased to 2000 cells/well, there was only an observed significant difference between the cells treated with 10 ng/mL of TGF-β1 compared to the control wells (1.28-fold increase, $p < 0.05$, **Figure 3B**). At a cell density of 3000 cells/well, there was a significant difference in cell counts between the control wells, and the wells treated with 5 ng/mL of TGF-β1 (1.2-fold increase, $p < 0.05$, **Figure 3B**) and 10 ng/mL of TGF- β1 (1.17-fold increase, $p < 0.05$, **Figure 3B**). At a cell density of 4000 cells/well, there was a significant difference in cell counts between the control wells, and 10 ng/mL of TGF-β1 treated wells (1.15-fold increase, $p < 0.05$, **Figure 3B**). Lastly, when the cell density reached 5000 cells/well there was only a significant decrease in the cells treated with 10 ng/mL TGF-β1 compared to the control (1.16-fold decrease, $p < 0.05$, **Figure 3B**).

In contrast to the Hoechst method, the CCK-8 methods display statistical increases in cell counts after treatment with TGF-β1 concentrations at higher cell densities like 4000, and 5000 cells per well (**Figure 3A**). However, in the Hoechst method statistical increases were observed when cell densities

were 2000, 3000, and 4000 cells per well. Furthermore, for CCK-8, wells seeded with 4000 cells showed increased proliferation at both 5 and 10 ng/mL of TGF-β1. However, Hoechst staining revealed a significant increase only at 10 ng/mL of TGF-β1 in wells with 4000 cells(**Figure 3**). In addition to this, for CCK-8, wells seeded with 5000 cells demonstrated a significant increase in cells at 10 ng/mL of TGFβ1 treatment. In contrast, Hoechst staining showed a significant decrease in cells relative to the control (**Figure 3**).

Altogether, this data supports that using lower cell densities in the Hoechst method significantly increases cells treated with TGF-β1 compared to the control. On the other hand, using higher cell densities in the CCK-8 method significantly increases cells treated with TGF-β1 compared to control. Furthermore, in this study Hoechst nuclear counting was designated as the primary endpoint of proliferation. This was done as the Hoechst method measures cell number whereas CCK8 assay is influenced by cellular metabolic changes.[28]

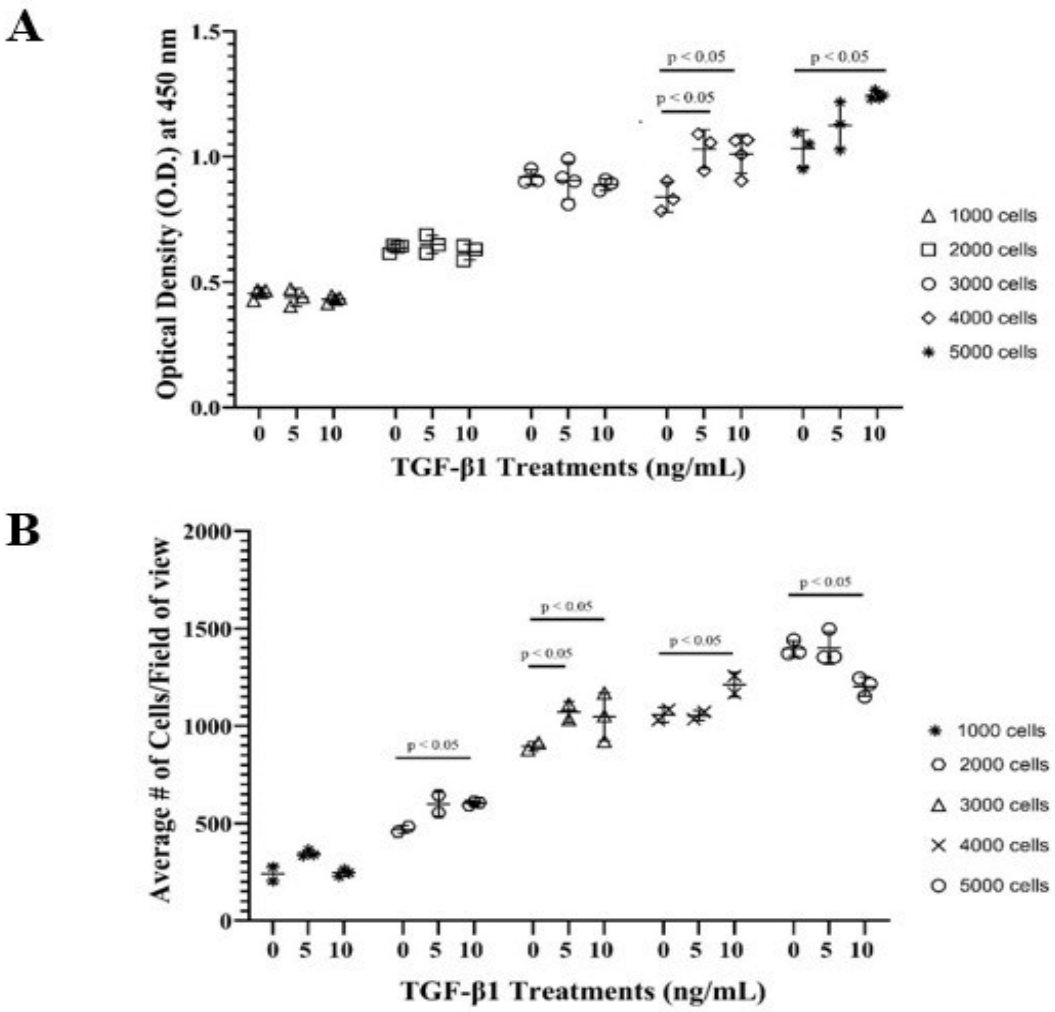

Figure 3. Optimization of TGF-B1 concentration for proliferation assays with human atrial fibroblasts. Human atrial fibroblasts were treated with increasing concentrations of TGF-β1 (5 and 10 ng/mL) for 48 hours to assess its effect on cell proliferation. **(A)** Proliferation was measured using the CCK-8 assay, with absorbance readings taken at 450 nm (n=3-4 technical replicates, n=1 biological replicate). Data is presented as mean absorbance ± standard deviation (SD). Two-way ANOVA with Tukey's post hoc test. Significant differences are shown as $p \leq 0.05$. **(B)** Cell counts were determined manually from Hoechst-stained cells using ImageJ (n = 2-3 technical replicates, n=1 biological replicate). Data are expressed as the mean cell number per field of view ± SD. Two-way ANOVA with Tukey's post hoc test. Significant differences are shown as $p \leq 0.05$.

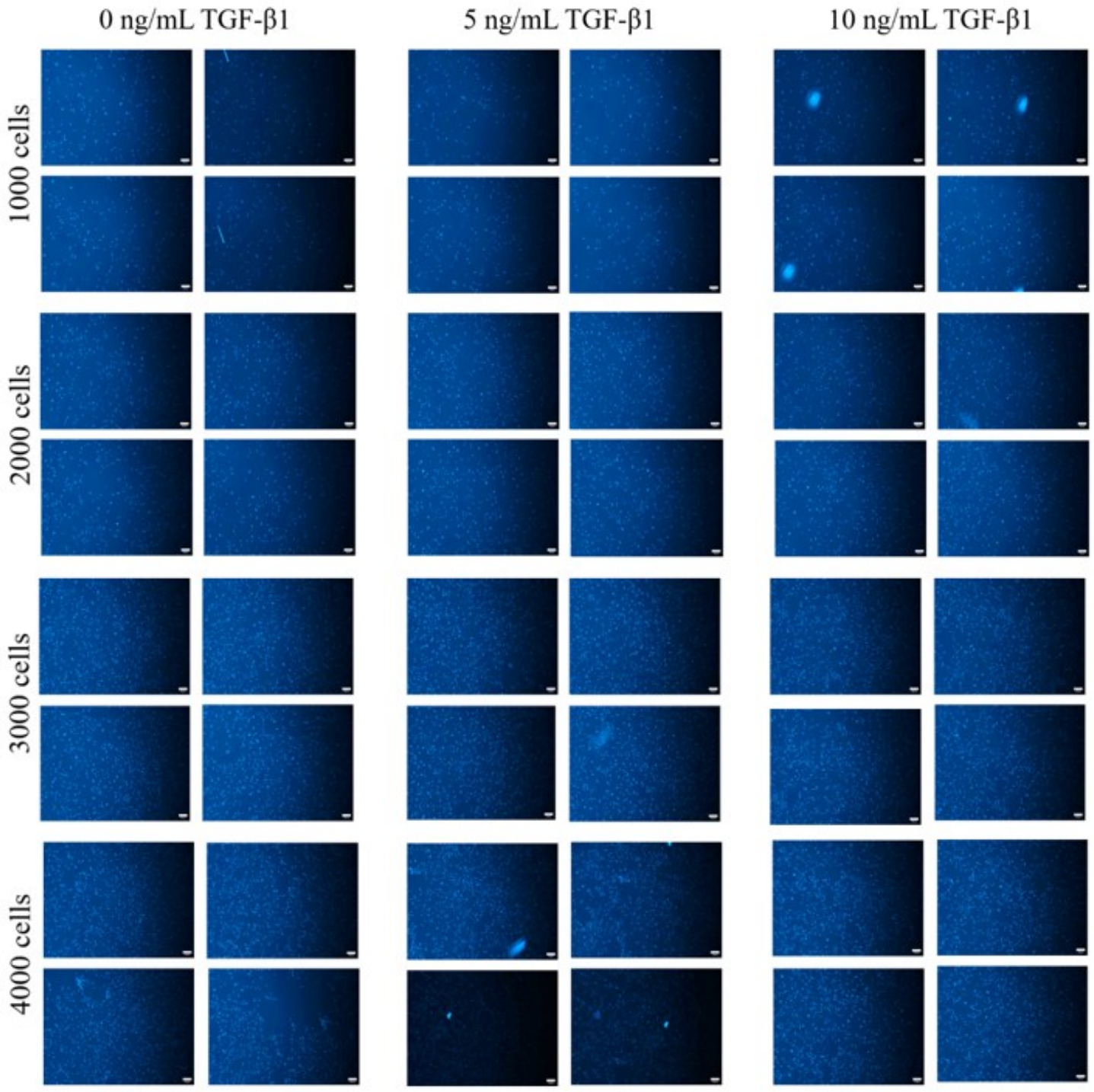

Figure 4. Hoechst images of human atrial fibroblasts. Fibroblasts were seeded at varying densities including 1000, 2000, 3000, and 4000 cells in a 96 well plate. Cells were treated with 0 ng/mL of TGF-β1 (n=1 technical replicate, n=1 biological replicate), 5 ng/mL of TGF-β1 (n=1 technical replicate, n=1

biological replicate), 10 ng/mL of TGF- β1 (n=1 technical replicate, n=1 biological replicate) for 48 hours. Fluorescent microscopy was used to capture images at 5x magnification that show the Hoechst-stained nuclei of the cells. The scale bar represents 100 μm.

Characterization of Extracellular Vesicles (EVs) and Decorin Localization

Extracellular vesicles were isolated multiple times to study the role of decorin and to conduct downstream experiments (**Figure 5A**). Nanoparticle Tracking Analysis (NTA) instrument was used to determine the size, and concentration of extracellular vesicles by creating a 60 second video of the sample (**Figure 5C**). NTA displays this data as a graph to demonstrate the relationship between the size of extracellular vesicles (nm) and the concentration of the sample (particles/ml) (**Figures 5B, 5D, and 5E**).

To explore variability between samples of extracellular vesicles, three independently prepared samples using the same protocol were analyzed for particle concentration and size. In the first sample of extracellular vesicles had a concentration of 4.37×10^{10} particles/ml (**Figure 5B**). The mean size of particles in this sample were (190.3 ± 97.1) nm, however the peaks generated by NTA demonstrate variability in particle size (**Figure 5B**). This graph consisted of four peaks, each peak represents a group of particles with similar diameters (**Figure 5B**). The first peak is the highest compared to the others and is located at 143 nm, whereas the following peaks were located at 232, 336, and 465 nm (**Figure 5B**). In the second sample of extracellular vesicles concentrated at 2.24×10^{10} particles/ml (**Figure 5D**). For this sample, the NTA data displayed three peaks (**Figure 5D**). The highest peak was observed at 88 nm, whereas the following peaks were observed at 125, and 194 nm (**Figure 5D**). The mean size of particles found in this sample were (103.2 ± 31.9) nm. Lastly, in the third sample of extracellular vesicles concentrated at 4.89×10^{10} particles/ml, five peaks were observed (**Figure 5E**). The highest peak was observed at 134 nm, whereas the other peaks were observed at 207, 339, 479, and 688 nm (**Figure 5E**). The mean size of particles in this sample is (222.5 ± 103.9) nm. Interestingly, these samples differed in terms of their concentration and size of extracellular vesicles.

To further investigate whether ultracentrifugation (UC) generated an optimal concentration of extracellular vesicle, a sample of fixed EVs was sent for transmission electron microscopy (TEM) to be negative stained. The images of extracellular vesicles were taken at the following magnifications: 20,000 x, 25,000 x, 30,000 x, 60,000 x, 80,000 x, and 100,000 x (**Figure 6**). The image taken at 20,000 x displays seven extracellular vesicles with a lipid bilayer, and cup-shaped morphology, (**Figure 6A**). According to the scale bar, the sizes of these EVs are about 70 – 100 nm. Notably, there are less extracellular vesicles (two) with about a diameter of 100, and 150 nm visualized in an image taken at 25,000 x magnification (**Figure 6B**). At 30,000 x magnification, there were less extracellular vesicles (two) visualized with about 80 nm, and 170 nm diameter compared to 20,000 x magnification (**Figure 6C**). Interestingly, at 60,000 x magnification, there were 3 extracellular vesicles with diameters of about 100, 110, and 200 nm within that field of view (**Figure 6D**). At 80,000 x magnification, four extracellular vesicles were observed with sizes 80 nm, 80 nm, 90 nm, and 100 nm (**Figure 6E**). Lastly, at the 100,000 x magnification, there was only one extracellular vesicle visualized with about 100 nm diameter (**Figure 6F**).

Extracellular vesicles were further processed using immunohistochemistry (IHC) to localize decorin within these molecules. Transmission electron microscopy (TEM) was used to capture images of a sample of EVs at the following magnifications: 50,000 x, 80,000 x, 100,000 x, 120,000 x, and 150,000 x magnification (**Figure 7**). At 50,000 x, there was an extracellular vesicle about 100 nm present with clusters of decorin surrounding its lipid bilayer (**Figure 7A**). At 150,000 x, the EVs have a diameter of about 50 nm (**Figure 7B and 7C**).

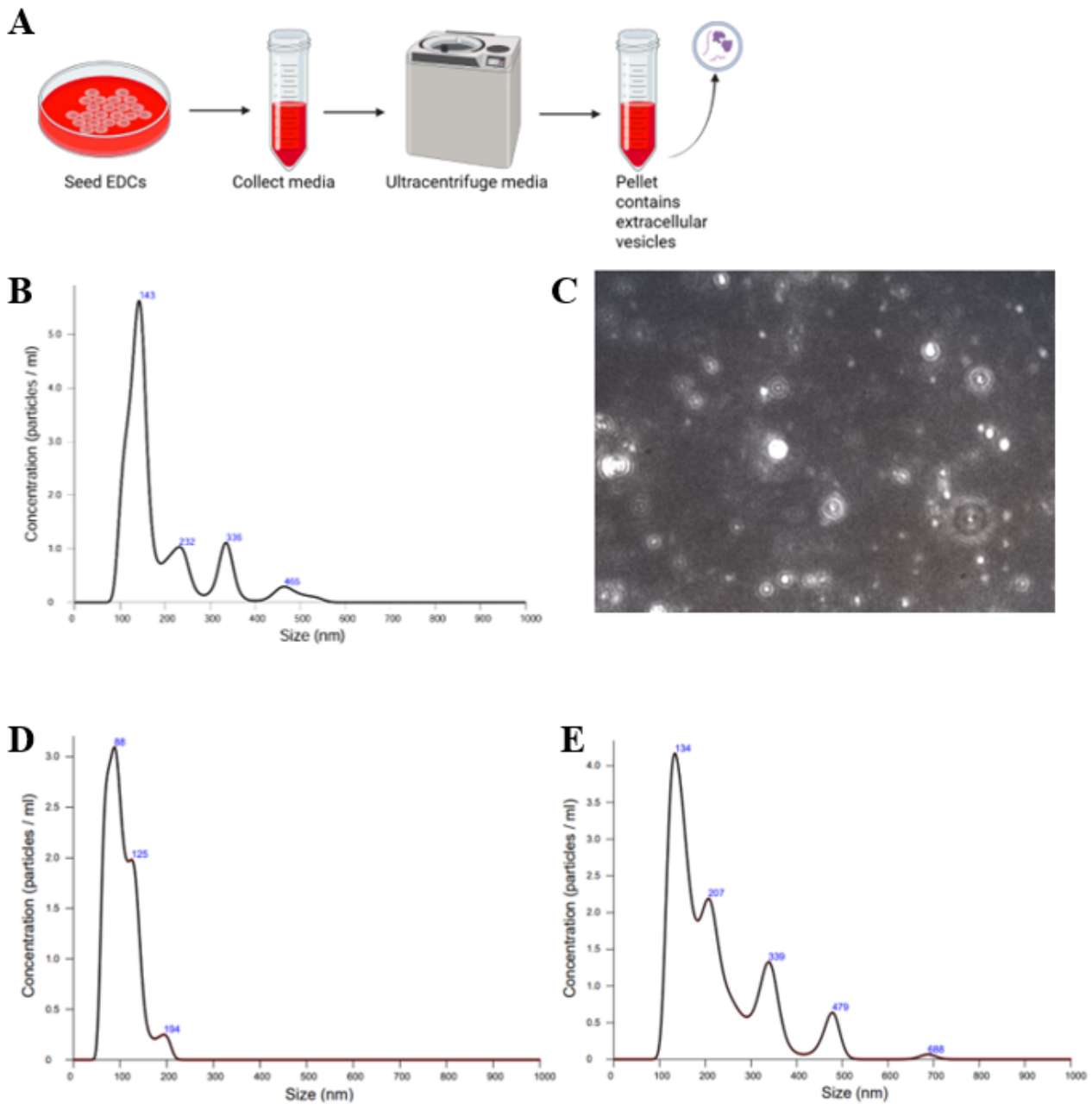

Figure 5. Isolation of Extracellular Vesicles from human explant derived cells (EDC). (A) Schematic overview of the extracellular vesicle isolation from EDCs conditioned media. **(B)** The Nanoparticle Tracking Analysis (NTA) instrument determines the concentration of the isolated EVs and displays the particle sizes within this sample **(C)** This image represents a single frame from a 60-second NTA video acquisition using the sample presented in (B). Individual extracellular vesicles (EVs) are visible as bright

points of scattered light, exhibiting Brownian motion within the sample volume. The software tracks the movement of these particles to determine their diameter and concentration. **(D)** NTA of a second extracellular vesicle sample shows particle concentration and size distribution. **(E)** NTA of a third EV sample's concentration and size distribution was measured. n=3 biological replicates, and n=1 technical replicate.

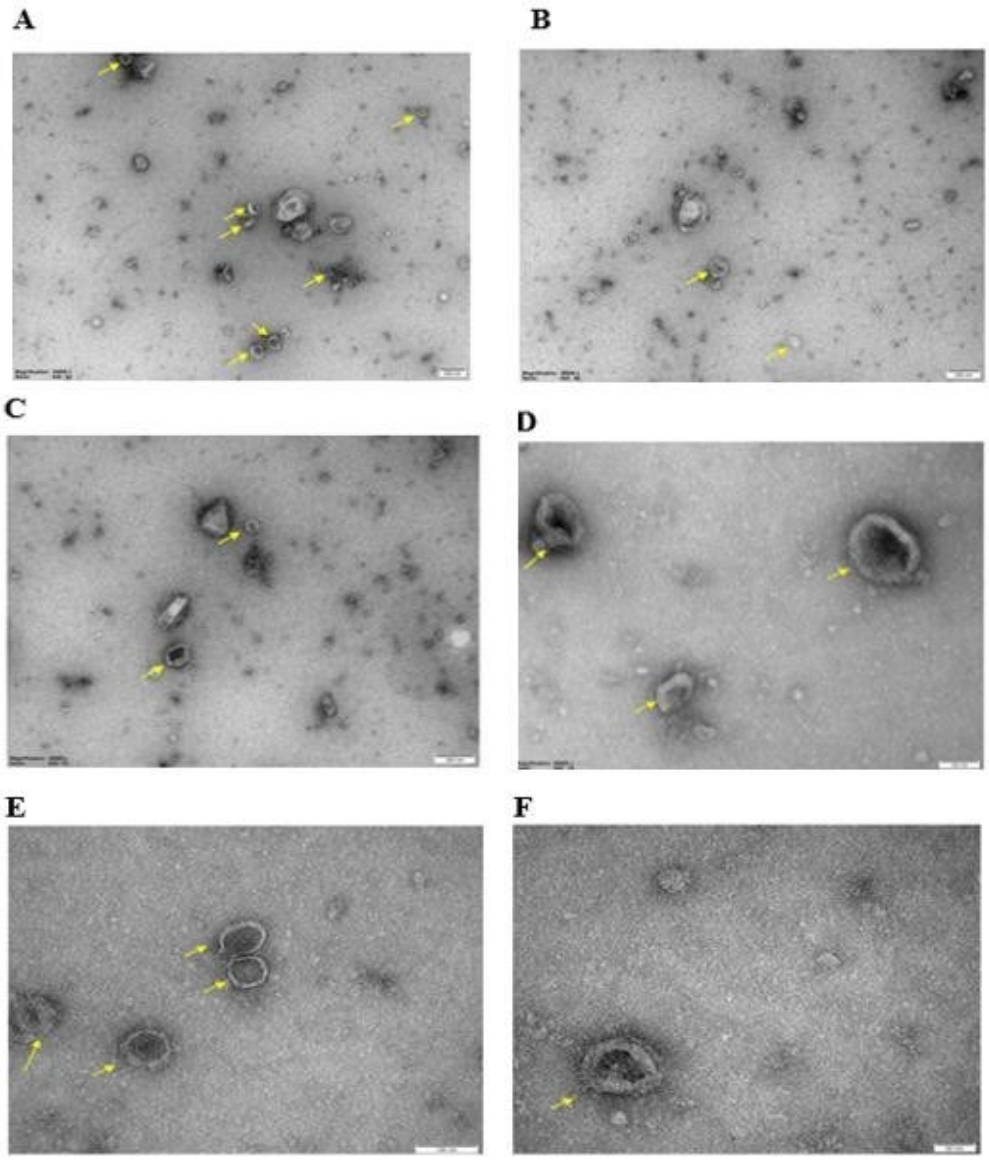

Figure 6. Transmission electron microscopy (TEM) imaging of extracellular vesicles. A transmission electron microscope was used to take images of a fixed extracellular vesicles sample at the following

magnifications: **(A)** 20,000 x (scale bar: 200 nm) **(B)** 25,000 x (scale bar: 200 nm) **(C)** 30,000 x (scale bar: 200 nm) **(D)** 60,000 x (scale bar: 100 nm) **(E)** 80,000 x (scale bar: 100 nm) **(F)** 100,000 x (scale bar: 50 nm). The yellow arrows were used to highlight extracellular vesicles within the above panels. The scale bars for each image is located in the bottom right corner. n=6 technical replicates, and n=1 biological replicate.

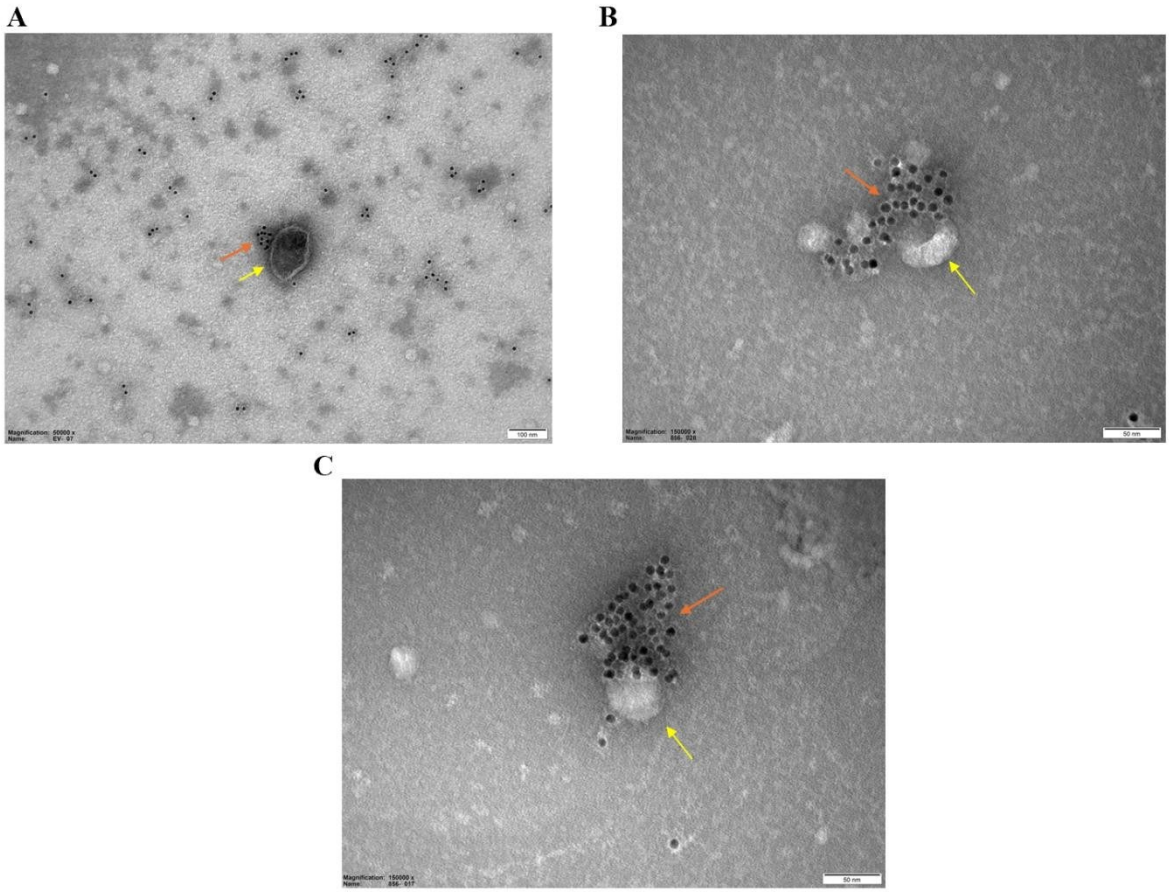

Figure 7. Transmission electron microscopy (TEM) imaging used to localize decorin within extracellular vesicles. To localize decorin images were taken at the following magnifications: **(A)** 50,000x magnification (scale bar: 100 nm) **(B)** 150,000x magnification (scale bar: 50 nm) **(C)** 150,000x magnification (scale bar: 50 nm) Yellow arrows highlight extracellular vesicles within these images, and orange arrows highlight decorin within these panels. n=2 biological replicates, and n=1-2 technical replicates per biological replicate.

siRNA – Mediated Depletion of Decorin in Extracellular Vesicles

To generate decorin depleted extracellular vesicles for downstream assays, knockdown was optimized and validated using quantitative polymerase chain reaction (qPCR), and enzyme-linked immunosorbent assay (ELISA). Extracellular vesicles were generated by plating about 400,000 – 600,000 human explant derived-cells (EDCs) on three petri dishes. The media from each petri dish was processed to collect 200 µL of extracellular vesicles. To prevent overconsumption of reagents, knockdown was initially performed on a smaller scale where 6, 12, and 24-well plates were used to optimize the number and concentration of siRNA, and lipofectamine reagent.

Knockdown was first attempted using a 6-well plate where the cells were treated for 24 hours using 10 nM of a DsiRNA and control mimic with lipofectamine 2000 reagent. qPCR was conducted using cell lysate, which demonstrated no significant difference between the control and treatment wells ($p > 0.05$, **Figure 8**). Moving forward, ELISA was incorporated into these knockdown experiments to confirm reduction of protein levels. To improve knockdown efficiency, cells in a 12-well plate were treated with two DsiRNA (20 nM each) for 72 hours with lipofectamine RNAiMAX. qPCR conducted using cell lysate revealed that there is no significant difference between control and treatment groups ($p > 0.05$, **Figure 9A**). However, ELISA revealed that there is a reduction in decorin in the treatment group compared to the control (2.7-fold decrease, $p<0.05$ **Figure 9B**). As there was no difference observed in the qPCR data, three siRNA (10 nM each) were used to treat cells for 72 hours. The qPCR data shows a significant reduction in *DCN* expression as compared to the control group (41-fold decrease, $p< 0.05$, **Figure 10A**). ELISA was conducted on the same cells conditioned media which also resulted in a significant decrease in decorin levels compared to the control group (39-fold decrease, $p < 0.05$, **Figure 10B**). Hence, optimization on a small scale demonstrated a reduction in protein levels and gene expression compared to control when cells were treated with 3 DsiRNA (10 nM each) for 72 hours.

On a large-scale knockdown of decorin, 3 DsiRNA (10 nM each), control mimic, and vehicle (lipofectamine RNAiMAX) were used to treat human explant-derived cells. A vehicle (lipofectamine RNAiMAX) treatment was used to ensure no residual transfection reagents in the EV sample. After 72 hours of treatment, the cell lysate and conditioned media were obtained. The cell lysate was used to analyze decorin expression using qPCR, which displayed a significant difference between control mimic and DsiRNA (208-fold decrease, $p<0.05$, **Figure 11A**). In addition to this, ELISA demonstrated that there was a significant decrease in decorin expression in extracellular vesicles treated with DsiRNA compared to treatment with control mimic (36-fold decrease, $p < 0.05$, **Figure 11B**) and vehicle (38-fold decrease, $p<0.05$, **Figure 11B**). ELISA had also shown that the EVs treated with vehicle consisted of 9.16×10^7 EVs/pg of DCN, EVs treated with control mimic consisted of 1.14×10^8 EVs/pg of DCN, EVs treated with DsiRNA consisted of 3.7×10^9 EVs/pg of DCN.

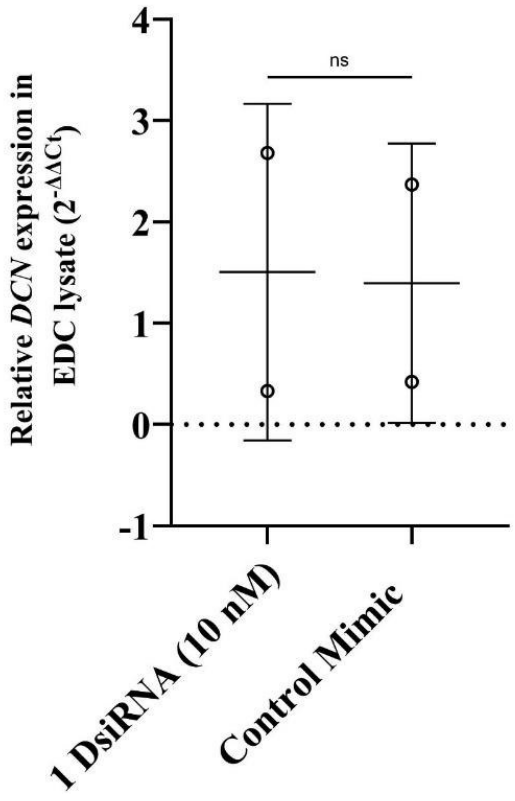

Figure 8. qPCR confirmation of decorin knockdown. Quantitative polymerase chain reaction (qPCR) was conducted on human explant-derived cells (EDC) cell lysate (n=2 technical replicates, n=1 biological

replicate). Human atrial fibroblasts seeded in a 6-well plate were treated with siRNA and control mimic for 24 hours. siRNA and control mimic treatment were facilitated using lipofectamine 2000 reagent. Values are shown as mean ± standard deviation (1 DsiRNA: 1.5 ± 1.7 and Control Mimic: 1.4 ± 1.4). Unpaired t-test was used to determine statistical difference between these groups ($p \leq 0.05$).

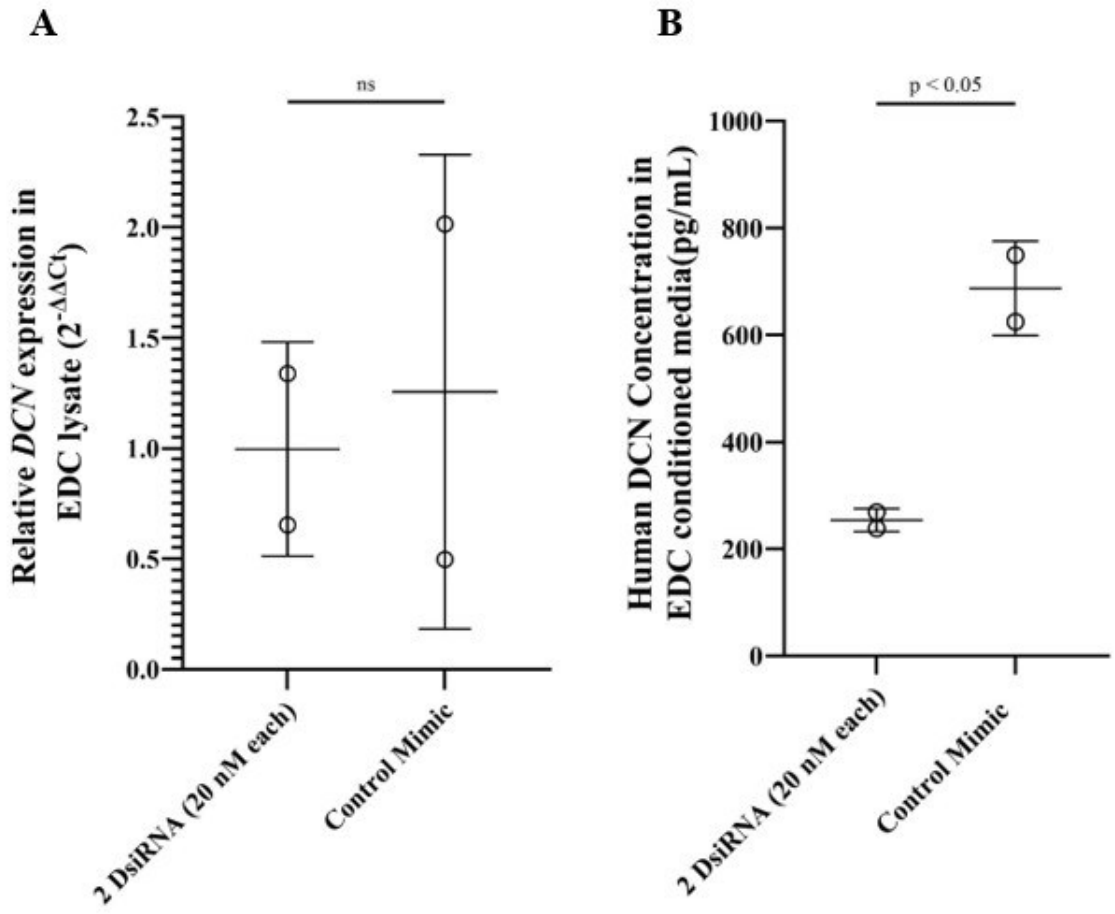

Figure 9. qPCR and ELISA confirmation of decorin knockdown. Human atrial fibroblasts were seeded in a 12-well plate and treated with 2 siRNA (20 nM each) and control mimic. The siRNA and control mimic treatment were facilitated using lipofectamine RNAiMAX reagent. **(A)** The cell lysate was obtained and used to conduct qPCR (n=2 technical replicates, n=1 biological replicate). Values are shown as mean ± standard deviation (2 DsiRNA: 0.99 ± 0.48 and Control Mimic: 1.25 ± 1.07). Unpaired t-test was used to determine statistical difference ($p \leq 0.05$) .**(B)** EDC conditioned media was used to conduct

ELISA to confirm protein level knockdown (n=2 technical replicates, n=1 biological replicate). Values are shown as mean ± standard deviation (2 DsiRNA: 253 ± 21.4 and Control Mimic: 687 ± 88). Unpaired test was used to determine statistical difference ($p \leq 0.05$).

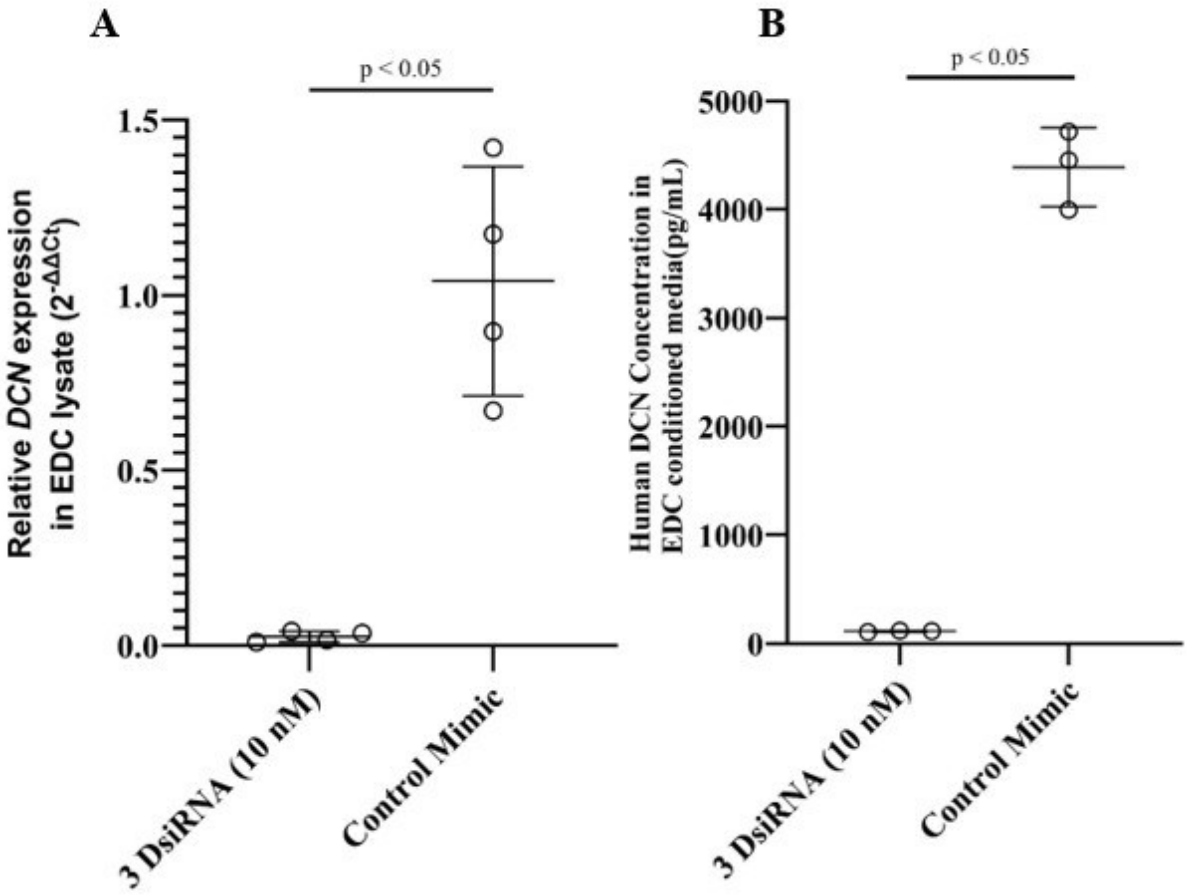

Figure 10. EDCs decorin knockdown using siRNA in a 24-well plate. These cells were seeded in a 24well plate and exposed to two treatments: control mimic, and decorin siRNA. **(A)** After 72 hours, qPCR was used to evaluate gene expression using cell lysate (n=4 technical replicates, n=1 biological replicate). Values are shown as mean ± standard deviation (3 DsiRNA: 0.025 ± 0.015 and Control Mimic: 1.04 ± 0.33). Unpaired t-test was used to determine statistical difference ($p \leq 0.05$). **(B)** After 72 hours, ELISA was used to determine decorin concentration within EDCs conditioned media (n=3 technical replicates, n=1 biological replicate). Values are shown as mean ± standard deviation (3 DsiRNA:111.76 ± 6.55 and Control Mimic: 4389.69 ± 364.61). Unpaired t-test was used to determine statistical difference ($p \leq 0.05$).

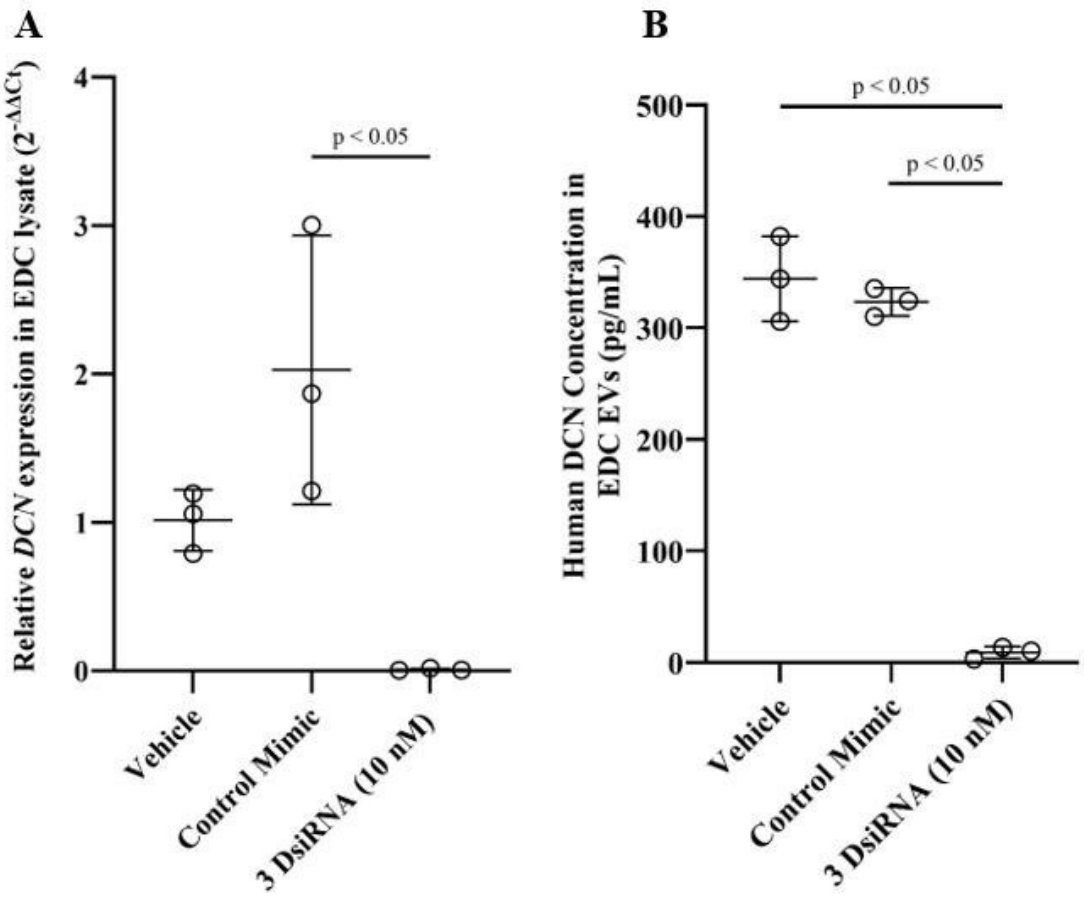

Figure 11. EDCs EVs depletion of decorin using siRNA in petri dishes. These cells were seeded in petri dishes and exposed to three treatments: vehicle, control mimic, and dsiRNA. After 72 hours, the EDCs conditioned media were processed to obtain extracellular vesicles (EVs), and the cell lysate was obtained. **(A)** After 72 hours, qPCR was used to evaluate gene expression using cell lysate (n=3 technical replicates, n=1 biological replicate). Values are shown as mean ± standard deviation (Vehicle: 1.01 ± 0.2, Control Mimic: 2.03 ± 0.9, and 3 DsiRNA: 0.0097 ± 0.007). One-way ANOVA with Tukey's post hoc test. **(B)** After 72 hours, ELISA was used to determine decorin's concentration within EDCs EVs (n=3 technical replicates, n=1 biological replicate). Values are shown as mean ± standard deviation (Vehicle: 344 ± 38, Control Mimic: 323 ± 12.56, and 3 DsiRNA: 8.96 ± 5.29). One-way ANOVA with Tukey's post hoc test.

Decorin Treatment Does Not Alter Cell Proliferation Relative to Controls

In vitro assays were performed by treating human atrial fibroblasts with decorin and TGF-β1. To assess whether decorin alone alters cell proliferation, separate wells treated with decorin or TGF-β1 individually prior to examining their combined effects. Cell proliferation was analyzed using the cell counting kit-8 (CCK-8), and Hoechst staining of nuclei. CCK-8 assay quantifies the metabolic activity of cells which is measured using a microplate reader at 450 nm.[29] On the other hand, Hoechst staining was used to stain nuclei, and four images of each well were taken using a fluorescent microscope.

The CCK-8 assay graph depicts a relationship between the following treatments administered to the cells: control (media), 1 µg/mL decorin, 10 µg/mL decorin, and TGFβ1 and the optical density measured at 450 nanometers (**Figure 12A**). This assay demonstrated that cells treated with only media had an average optical density (OD) of (0.78 ± 0.05) at 450 nm. Cells treated with 1 µg/mL and 10 µg/mL decorin had an average optical density (OD) of (0.791 ± 0.036), and (0.743 ± 0.044) like the control values ($p > 0.05$, **Figure 12A**). However, cells treated with TGF-β1 displayed an average optical density of (1.038 ± 0.072) at 450 nm, significantly higher than cells treated with media (95% CI of difference: 0.39 to -0.12,1.33-fold increase, $p < 0.05$, **Figure 12A**), 1 µg/mL decorin (95% CI of difference: -0.38 to 0.11, 1.31-fold increase, $p < 0.05$, **Figure 12A**), and 10 µg/mL decorin (95% CI of difference: -0.43 to -0.16,1.4-fold increase, $p < 0.05$, **Figure 12A**).

In contrast, **Figure 12B** illustrates a relationship between the various cell treatments: control (media), 1 µg/mL decorin, 10 µg/mL decorin, and TGFβ1 and the average number of nuclei stained using Hoechst per field of view. Cells treated with TGF-β1 had (2758 ± 313) nuclei per field of view. This was significantly higher than wells treated with media (95% CI of difference: -1224 to -293, 1.38-fold increase, $p < 0.05$, **Figure 12B**), and 1 µg/mL decorin (95% CI of difference: -1079 to -148, 1.29-fold increase, $p < 0.05$, **Figure 12B**). Interestingly, a non-significant upward trend was observed between cells

treated with 10 µg/mL decorin and TGF-β1 ($p < 0.05$, **Figure 12B**). Similarly, these trends are observed in representative Hoechst-stained images (**Figure 13, Supplementary Figure S2**). Cells treated with media visually have less Hoechst-stained nuclei as compared to those treated with TGF-β1 (**Figures 13A and 13B**). However, cells treated with 1 and 10 µg/mL of decorin visually have less stained nuclei compared to the cells treated with media (**Figures 13A, 13C, and 13D**).

These findings support that cells treated with varying concentrations of decorin do not alter cell proliferation compared to cells treated with TGF-β1.

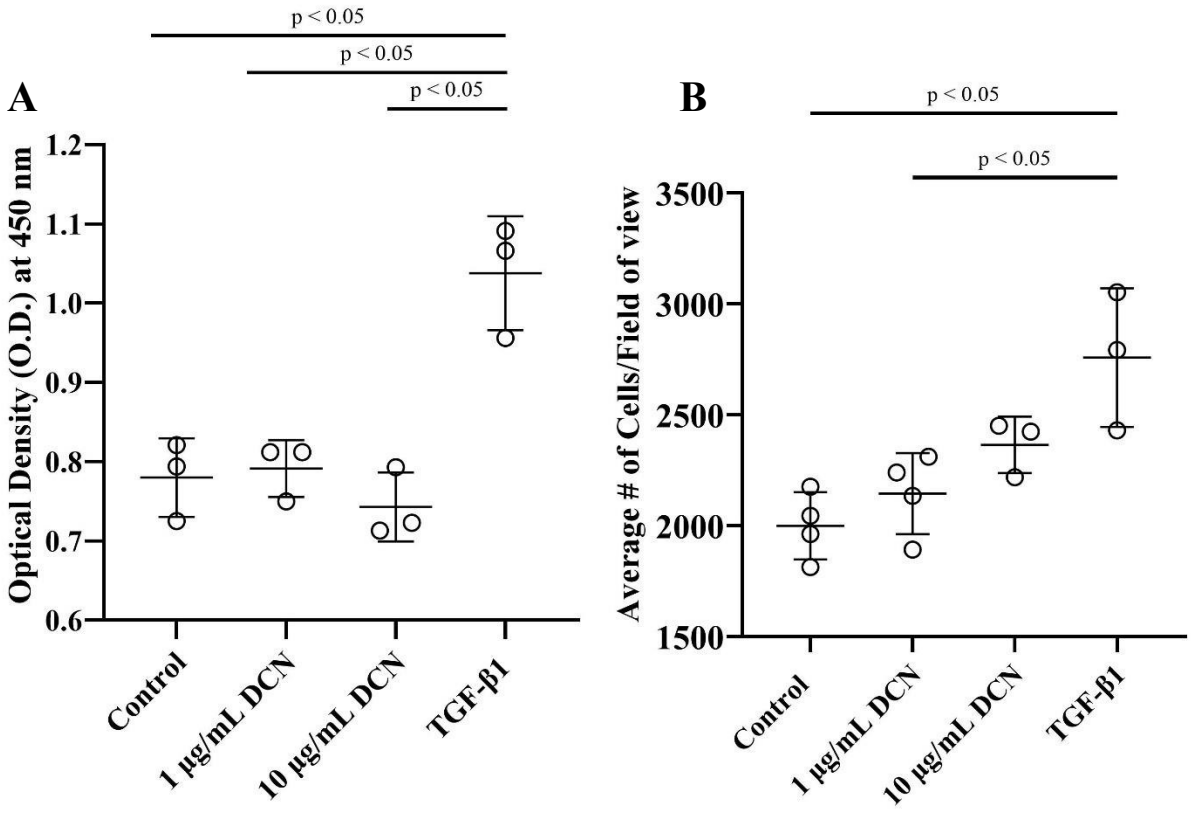

Figure 12. DCN has no effect on cell proliferation. Human atrial fibroblasts were seeded in 96-well plates. After 24 hours of seeding, these cells were treated with 1 µg/mL DCN, 10 µg/mL DCN, and TGFβ1 (10 ng/mL). **(A)** After 48 hours of treatment, cells proliferation was assessed using cell counting

kit-8 (CCK-8) (n=3 technical replicates, n=1 biological replicate). This dye is added to the wells consisting of cells and incubated. The optical densities are measured using a microplate reader. Values are shown as mean ± standard deviation (Control: 0.78 ± 0.05, 1 µg/mL DCN: 0.79 ± 0.04 ,10 µg/mL DCN: 0.743 ± 0.04, TGF-β1: 1.04 ± 0.07). One-way ANOVA with Tukey's post hoc test. Significant differences are shown as $p \leq 0.05$. **(B)** After 24 hours of treatment, cell proliferation was assessed using Hoechst staining (n=3-4 technical replicates, n=1 biological replicate). The stained nuclei within the wells are imaged using a fluorescent microscope at 365 nm filter. The nuclei were counted using ImageJ. Values are shown as mean ± standard deviation (Control:1999.5 ± 151.5, 1 µg/mL DCN: 2144.875 ± 182. 9,10 µg/mL DCN: 2364.58 ± 127.2, TGF-β1: 2758.16 ± 312.6). One-way ANOVA with Tukey's post hoc test. Significant differences are shown as $p \leq 0.05$.

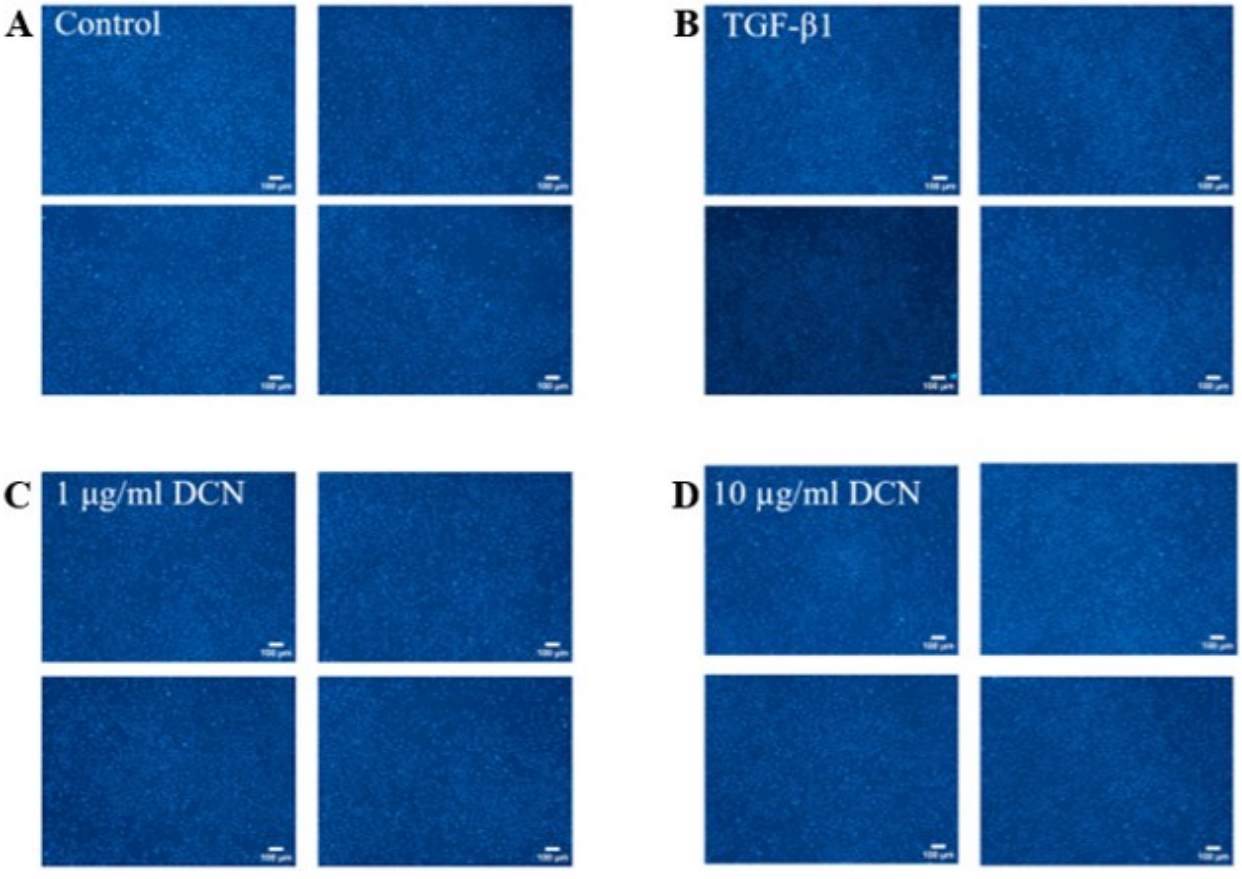

Figure 13. Hoechst-stained images of a well seeded human atrial fibroblasts separately treated with DCN and TGF-β1. Human atrial fibroblasts were seeded in a 96-well plate. After 24 hours, these cells

were treated separately with **(A)** media (n=1 technical replicate, n=1 biological replicate) **(B)** TGF-β1 (10 ng/mL) (n=1 technical replicate, n=1 biological replicate) **(C)** 1 µg/mL DCN (n=1 technical replicate, n=1 biological replicate) **(D)** 10 µg/mL DCN (n=1 technical replicate, n=1 biological replicate). After 24 hours of treatment, wells were treated with Hoechst to stain nuclei. Four images of each well were captured using a fluorescent microscope at a 5 x magnification. In this figure, one well with each treatment was illustrated but the other wells are shown in the supplementary figures. The nuclei were counted using ImageJ. The scale bar represents 100 µm.

Decorin inhibits TGF-β1- Induced Cell Proliferation

To investigate the relationship between decorin and TGF-β1, human atrial fibroblasts were cotreated with both proteins. Cell proliferation was assessed using CCK-8 assay, and Hoechst-stained nuclei. CCK-8 data depicts a relationship between the cell treatments: media (control), 1 µg/mL decorin with TGF-β1, 10 µg/mL decorin with TGF-β1, and TGF-β1 and the optical density measured at 450 nm. Cells treated with media (control) had an average optical density of (0.731 ± 0.021). It was observed that cells co-treated with 1 µg/mL decorin and TGF-β1 had an average optical density of (0.76 ± 0.046) which wasn't statistically different than the control group ($p < 0.05$, **Figure 14A**). Similarly, it was observed that cells co-treated with 10 µg/mL decorin and TGF-β1 had an average optical density of (0.728 ± 0.022) resulting in no significant difference than the control ($p < 0.05$, **Figure 14A**). However, TGF-β1 treated cells had an optical density of (0.887 ± 0.043) which was significantly higher than the control (95% CI of difference; -0.24 to -0.07, 1.21-fold increase, $p < 0.05$, **Figure 14A**).

To corroborate these findings, Hoechst-stained nuclei images were taken using a fluorescent microscope (**Figure 15, Supplementary Figure S3**). There were four pictures taken of each well, which were quantified using ImageJ (**Figure 15**). These images revealed that the average number of nuclei per field of view was comparable between media-treated, 1 µg/mL decorin and TGF-β1, and 10 µg/mL decorin and TGF-β1. Media- treated (control) wells had an average number of (3521± 303) cells per field of view, 1 µg/mL decorin and TGF-β1 had an average number of (3210 ± 322) cells per field of view, and

10 µg/mL decorin and TGF-β1 had an average number of (3403 ± 160) cells per field of view (**Figure 14B**). In contrast to this, **Figure 15B** depicts that wells treated with TGF-β1 visibly have a greater number of nuclei compared to the other treatments. This visual observation is confirmed with the quantitative analysis displayed in **Figure 14B.** Wells treated with TGF-β1 had an average of (4360 ± 105) cells per field of view which were significantly more than wells treated with media (95% CI of difference: -1344 to -334, 1.24-fold increase, $p < 0.05$) , 1 µg/mL decorin and TGF-β1 (95% CI of difference: -1656 to -646, 1.36-fold increase, $p < 0.05$), and 10 µg/mL decorin and TGF-β1 (95% CI of difference: -1463 to -453, 1.28-fold increase, $p < 0.05$). Wells treated with 1 µg/mL decorin with TGF-β1 had similar number of nuclei as wells treated with 10 µg/mL decorin with TGF-β1 ($p > 0.05$, **Figure 14B**). This was also reflected visually in **Figures 15C and 15D**, which displayed similar numbers and distribution of nuclei in these wells.

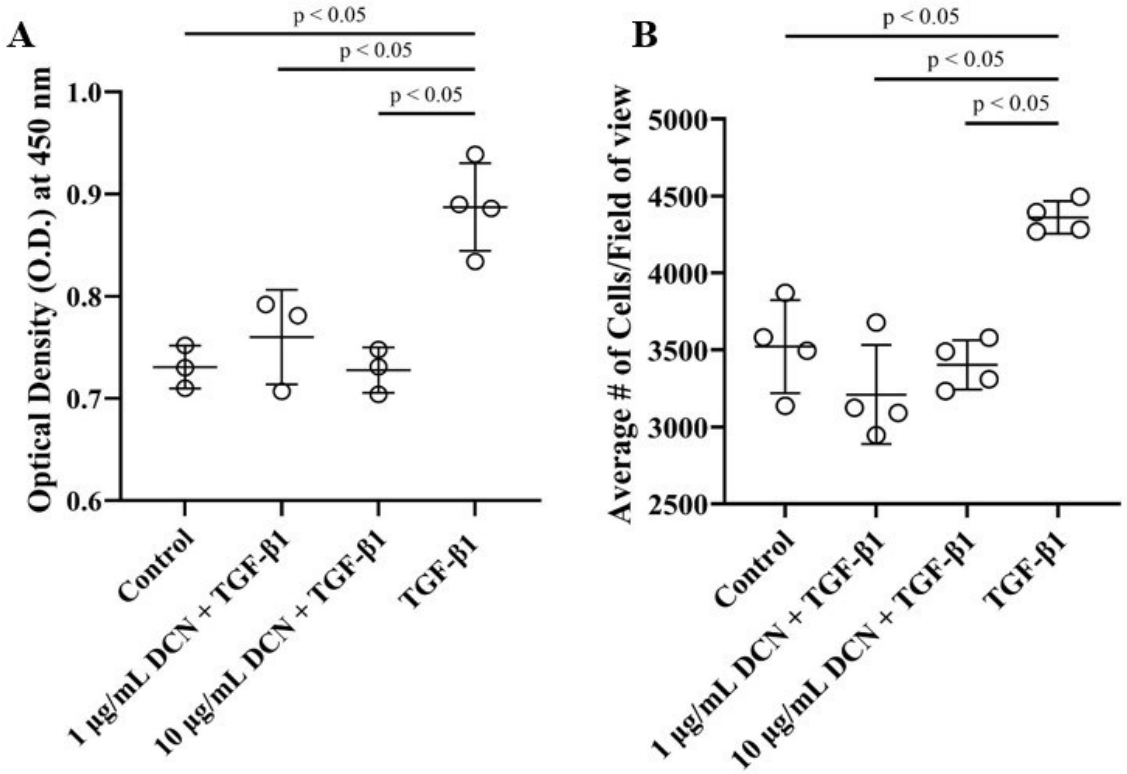

Figure 14. DCN inhibits TGF-β1 proliferative activity. Human atrial fibroblasts were seeded in 96-well plates. 24 hours later, these cells were treated with 1 µg/mL DCN and 10 µg/mL DCN. After 24 hours of

decorin treatment, these cells were treated with TGF-β1 (10 ng/mL). **(A)** After 48 hours of treatment, cell proliferation was assessed using cell counting kit-8 (CCK-8) (n=3-4 technical replicates, n=1 biological replicate). The optical density was measured at 450 nm using a microplate reader. Values are shown as mean ± standard deviation (Control: 0.73 ± 0.02, 1 µg/mL DCN + TGF-β1: 0.76 ± 0.05,10 µg/mL DCN + TGF-β1: 0.73 ± 0.02, TGF-β1: 0.89 ± 0.04). One-way ANOVA with Tukey's post hoc test. Significant differences are shown as $p \leq 0.05$. **(B)** After 24 hours of treatment, cell proliferation was measured using Hoechst staining (n=4 technical replicates, n=1 biological replicate). The wells containing the cells where imaged using a fluorescent microscope at a 365 nm filter. The nuclei were counted using ImageJ. Values are shown as mean ± standard deviation (Control: 3521 ± 302.5, 1 µg/mL DCN + TGF-β1: 3209.8 ± 321.67, 10 µg/mL DCN + TGF-β1: 3402.56 ± 159.58, TGF-β1: 4360.375 ± 105.4). One-way ANOVA with Tukey's post hoc test. Significant differences are shown as $p \leq 0.05$.

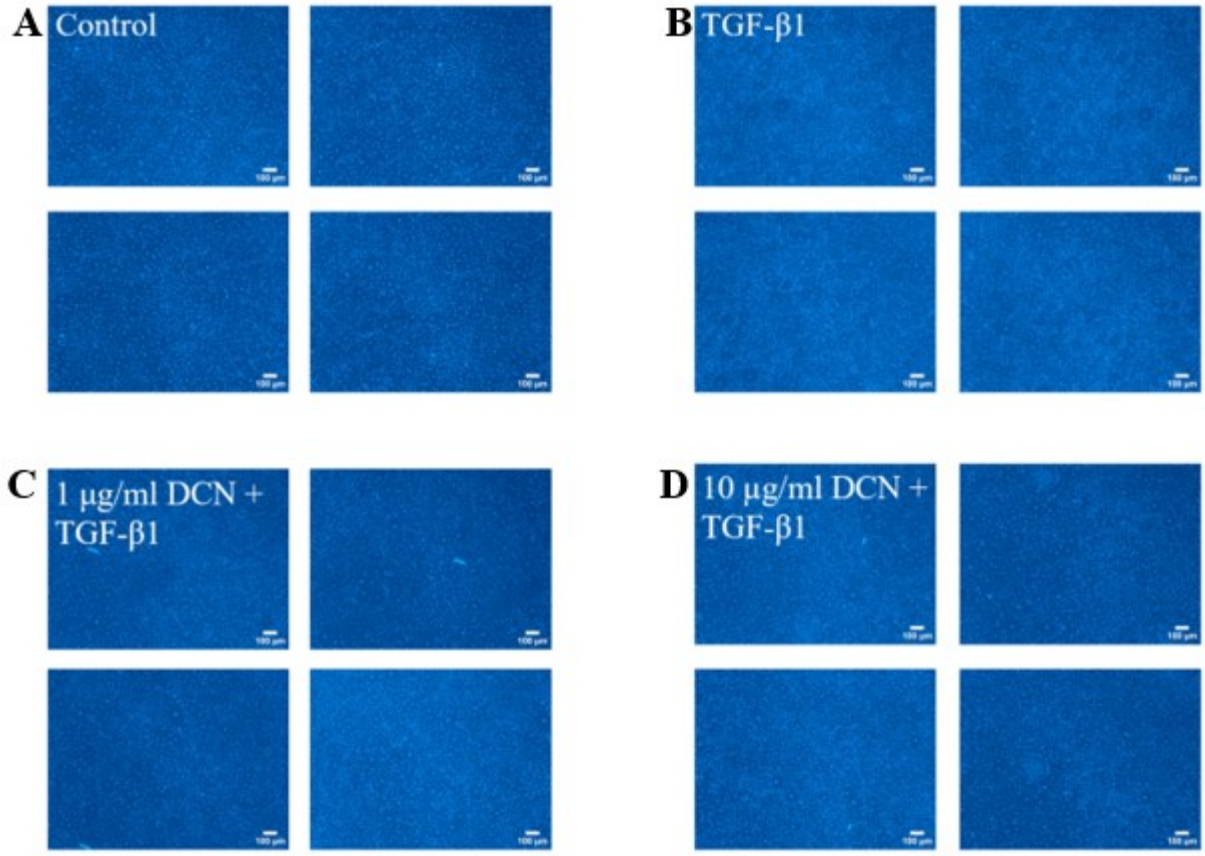

Figure 15. Hoechst-stained images of human atrial fibroblasts co-treated with DCN (1 µg/mL or 10 µg/mL) and TGF-β1 (10 ng/mL). Cells are seeded on 96-well plates. These cells are treated with **(A)**

media (n=1 technical replicate, n=1 biological replicate) **(B)** TGF-β1 (n=1 technical replicate, n=1 biological replicate) **(C)** 1 μg/mL decorin with TGF-β1(n=1 technical replicate, n=1 biological replicate) **(D)** 10 μg/mL decorin with TGF-β1 (n=1 technical replicate, n=1 biological replicate). 24-hour post-treatment, wells were treated with Hoechst to stain the nuclei. The wells were imaged using a fluorescent microscope and nuclei were counted using ImageJ. In this figure, one well per treatment is displayed, and the remaining wells are shown in the supplementary figures. The scale bar represents 100 μm.

Decorin-Enriched EVs Inhibit TGF-β1-Induced Proliferation

To test the effect of decorin-enriched and decorin-depleted extracellular vesicles on TGF-β1induced cell proliferation, I performed large-scale knockdown experiments using DsiRNA. The size, and concentration of these extracellular vesicles were determined using the NTA instrument. **Figures 16A and 16B** illustrate snapshots of a 60-second video that the NTA prepares to measure concentration of extracellular vesicles. These videos determined that the decorin-depleted sample consisted of 8.79×10^{10} EV particles/ml whereas the decorin-enriched EVs consisted of 7.42×10^{10} EV particles/ml. Majority of the decorin-depleted samples consisted of EVs with 140 nm diameter, which was less than the mean of this sample (176 ± 82.3) nm. Interestingly, **Figure 16C** depicts multiple peaks demonstrating that the decorin-depleted EV sample consists of particles of the following sizes: 111, 140, 288, 401, 511, and 929 nm. In contrast to this, decorin-enriched EV samples mainly had a 116 nm diameter, which was less than the average particle size within this sample of (166.4 ± 72.5) nm. In addition to this, **Figure 16D** depicts that this sample of EVs had multiple peaks representing particles in this sample with the following sizes: 116, 149, 282, 465, and 669 nm.

A ratio of 10,000 decorin enriched and depleted EVs per cell was used to treat cells prior to TGFβ1. This shows that EV dosage was normalized by particle number. These experiments were conducted twice to be analyzed by CCK8 and Hoechst staining (**Figure 18, Supplementary Figure S4**). **Figure 17A** shows that there was no significant difference between the cells treated with media and

decorin enriched EVs ($p > 0.05$). Similarly, in **Figure 17B** there was no significant difference between cells treated with media and decorin enriched EVs ($p > 0.05$). However, the optical density of cells treated with decorin depleted EVs were significantly higher than cells treated with media in the CCK8 assay (95% CI of difference: -0.22 to -0.03, 1.08-fold increase, $p < 0.05$, **Figure 17A**) and the Hoechst staining (95% CI of difference: -35 to -6.1, 1.23 fold-increase, $p < 0.05$, **Figure 17B**). There is a greater increase in Hoechststained nuclei in cells treated with decorin depleted EVs as compared to cells treated with decorin enriched EVs treatment (95% CI of difference: -45 to -16.1, 1.39 fold-increase, $p < 0.05$, **Figure 17B**). On the other hand, there isn't a significant increase in the optical density of cells treated with decorindepleted EVs compared to decorin-enriched EVs ($p > 0.05$, **Figure 17A**). Lastly, both assays have demonstrated there is no significance between cells treated with depleted decorin EVs and TGFβ1 ($p > 0.05$, **Figures 17A and 17B**).

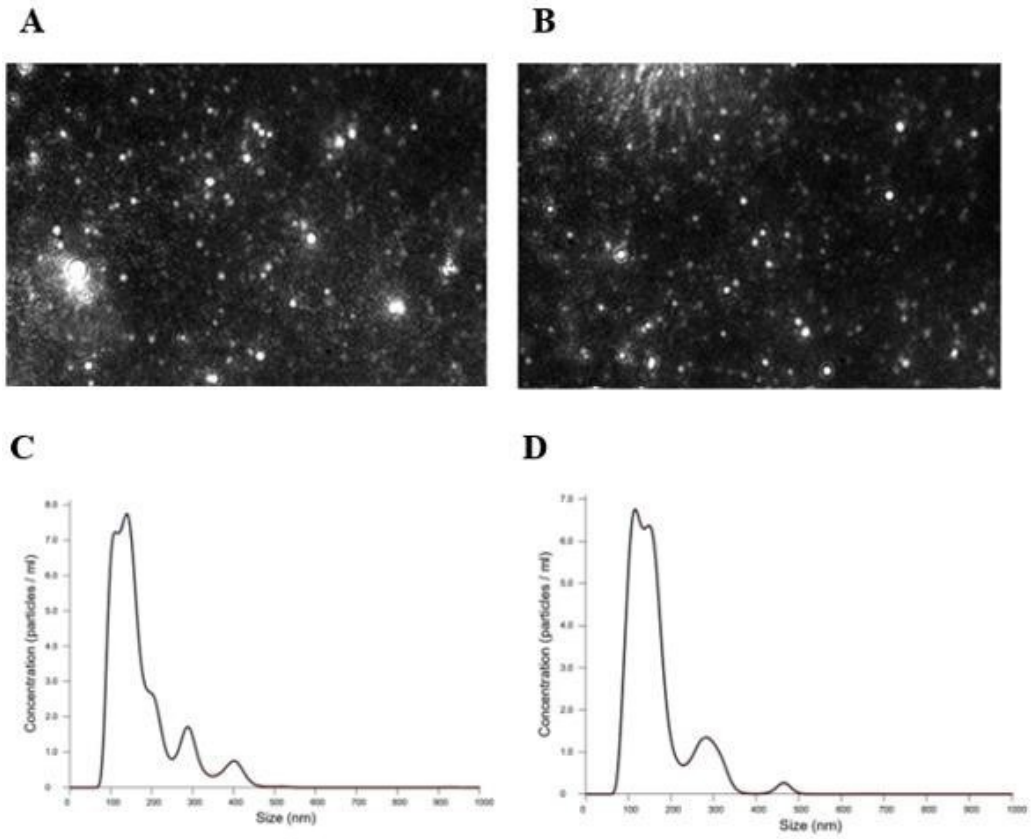

Figure 16. **NanoSight Tracking Analysis of decorin-enriched and decorin-depleted EVs. (A)** This image represents a single frame from a 60-second NTA video acquisition of the DsiRNA EV sample. **(B)**

This image represents a single frame from a 60-second NTA video acquisition of the control mimic EV sample. n=1 biological replicate, and n=1 technical replicate. **(C)** This histogram represents the nanosight data for the DsiRNA EV sample. n=1 biological replicate, and n=1 technical replicate. **(D)** This histogram represents the nanosight data for the Control Mimic EV sample.

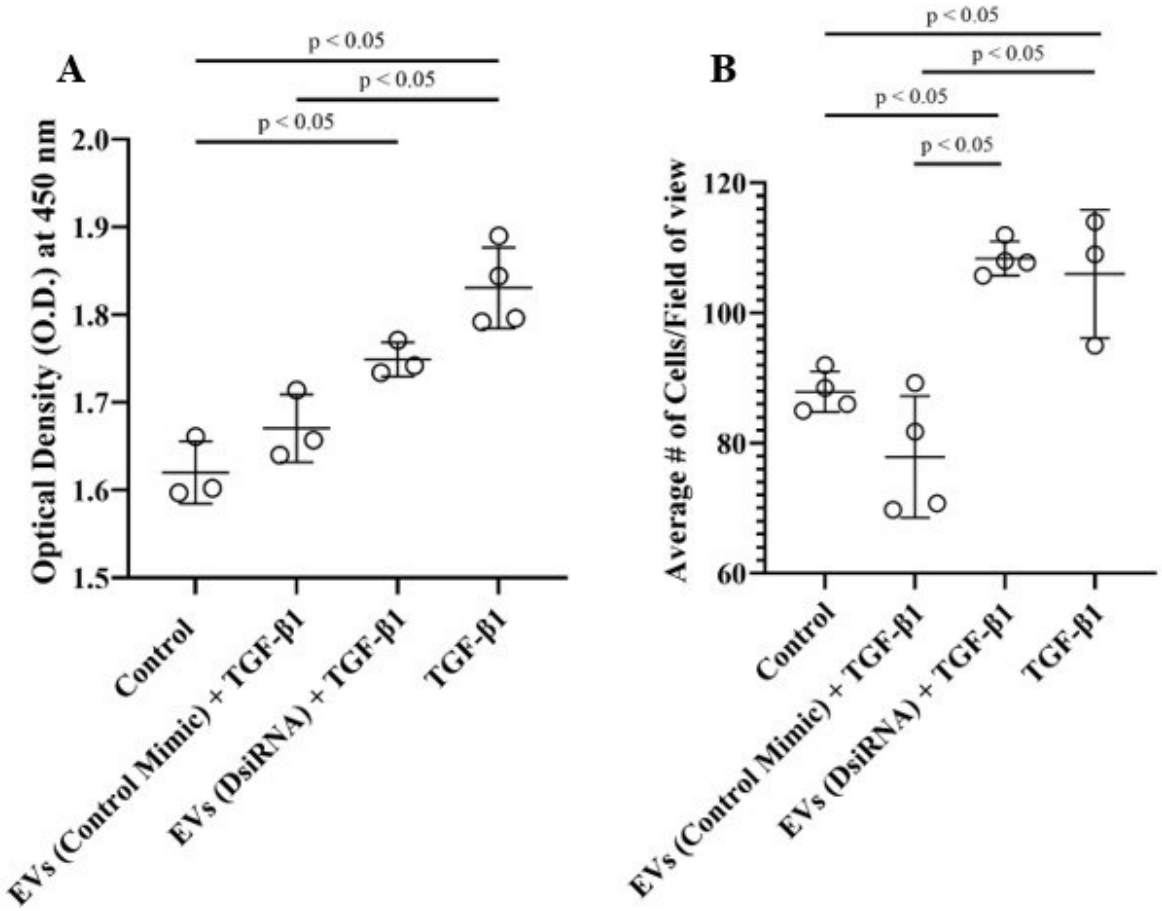

Figure 17. EVs depleted of decorin do not prevent TGF-β1 induced cell proliferation. Human atrial fibroblasts were seeded in 96-well plates. After 24 hours of seeding, cells were treated with decorin enriched and decorin-depleted EVs. A ratio of 10,000 EVs per human atrial fibroblast was used to normalize decorin-enriched and depleted EVs. After 24 hours, EV treated cells were exposed to TGF-β1 treatment. **(A)** After 48 hours of treatment, CCK-8 reagent was added into each well. The optical density of these wells was measured at 450 nm (n=3-4 technical replicates, n=1 biological replicate). Values are

shown as mean ± standard deviation (Control: 1.62 ± 0.04, EVs (Control Mimic): 1.67 ± 0.04, EVs (DsiRNA) + TGF-β1: 1.75 ± 0.02, TGF-β1: 1.8305 ± 0.05). One-way ANOVA with Tukey's post hoc test. Significant differences are shown as $p \leq 0.05$. **(B)** After 24 hours of treatment, Hoechst staining was used to stain cells nuclei (n=3-4 technical replicates, n=1 biological replicate). These cells were imaged using a fluorescent microscope at 365 nm filter. The nuclei were counted using ImageJ. Values are shown as mean ± standard deviation (Control: 87.875 ± 3.12, EVs (Control Mimic): 77.875 ± 9.33, EVs (DsiRNA) + TGF-β1: 108.375 ± 2.62, TGF-β1: 106 ± 9.85). One-way ANOVA with Tukey's post hoc test. Significant differences are shown as $p \leq 0.05$.

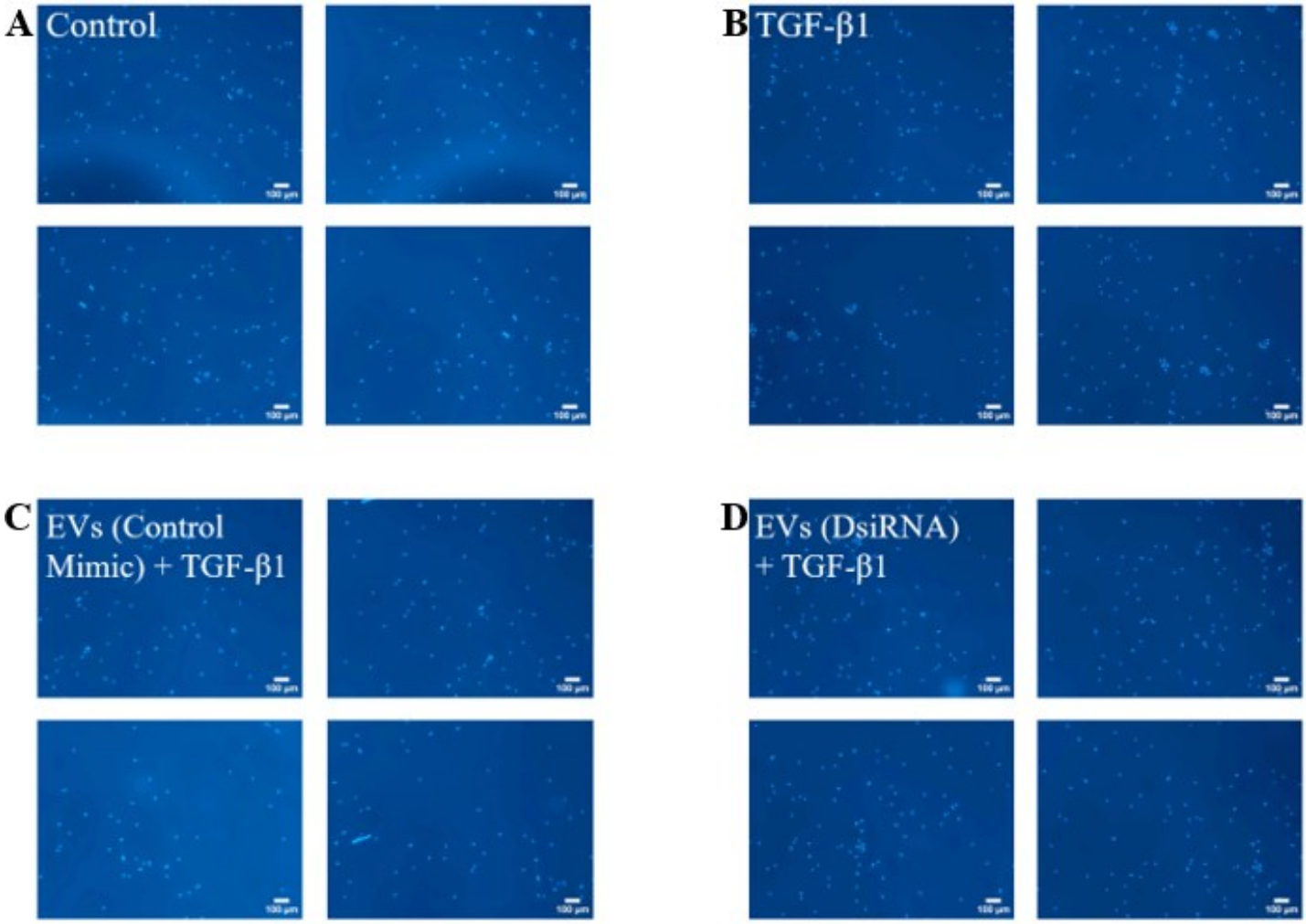

Figure 18. Hoechst-stained images of human atrial fibroblasts co-treated with extracellular vesicles and TGF-β1. Human atrial fibroblasts were seeded in 96-well plates. These cells were treated with **(A)**

media (n=1 technical replicate, n=1 biological replicate) **(B)** TGF-β1 (n=1 technical replicate, n=1 biological replicate) **(C)** EVs (control mimic) with TGF-β1 (n=1 technical replicate, n=1 biological replicate), and **(D)** EVs (DsiRNA) with TGF-β1(n=1 technical replicate, n=1 biological replicate). 24 hours later, Hoechst was added into each well to stain the nuclei. The nuclei were imaged using a fluorescent microscope. The scale bar represents 100 μm.

Discussion

There remains a need to develop therapies for post-operative atrial fibrillation (POAF). Current clinical therapies like β-Blockers and Amiodarone have adverse effects including bradycardia, hypotension, increases in liver enzymes, and thyroid dysfunction.[30,31] This demonstrates that there is a critical need for a novel and safe therapy. Extracellular vesicles (EVs) have been investigated by researchers due to their properties like low toxicity, and minor immunogenicity.[32] In addition to this, they participate in cardiovascular pathology and play a role in facilitating communication between cells like cardiomyocytes, fibroblasts, smooth muscle cells, and endothelial cells.[33] In particular, EVs generated in our lab are involved in reducing atrial fibrosis, atrial inflammation, and atrial fibrillation in a rat model.[34] These EVs were investigated further using proteomic analysis, which determined that their cargo highly expresses decorin, an antifibrotic protein.[7] Decorin is a small leucine-repeat proteoglycan (SLRP) that can inhibit TGF-β1 fibrotic potential.[35,36] This study was conducted to investigate whether decorin can reduce TGF-β1- induced proliferation of human atrial fibroblasts. The findings of this study determined that decorin itself and decorin enriched extracellular vesicles suppressed TGF-β1 induced fibroblast proliferation, suggesting decorin may be contributing towards EVs anti-fibrotic properties.

To explore the role of decorin within extracellular vesicles, an in vitro model of human atrial fibroblast induced proliferation was established. The results of this experiment show that the proliferation response was consistently dependent on both TGF-β1 concentration and cell-density. This was consistently seen in previous studies, in which higher concentrations of TGF-β1 can lead to scarring (fibrosis) whereas lower concentrations lead to minimal fibrosis.[37] Studies further demonstrated that a concentration-dependent proliferation was observed in cells like airway smooth muscle cells (ASMC) treated with various concentrations of TGF-β1 (0.1, 1, and 5 ng/mL).[38] In the context of the heart, TGF-β1 was demonstrated to increase fibroblast activity, involved in atrial fibrosis.[39] While, a general concentration-dependent trend was noted in the CCK8 and Hoechst assays in this study, a decrease in cell

counts were noted at a higher density of cells (like 5000 cells/well). This was highlighted in previous studies, as proliferation of fibroblasts was observed to be space constrained in vitro despite being treated by growth factors.[40] Based on this, a seeding density of 4000 cells/well were used in these assays. In addition to this, Hoechst staining was the primary proliferation endpoint whereas CCK8 was a secondary proliferation endpoint. Hoechst staining is stains the DNA of cells, therefore this method isn't dependent on the metabolism of cells unlike CCK8, therefore making Hoechst a suitable primary endpoint for proliferation.[41]

After establishing an in vitro model, the effect of decorin was investigated. This study demonstrated that decorin mediates the anti-fibrotic effects of extracellular vesicles (EVs). Decorin contributes to anti-fibrosis by binding to TGF-β1.[42] This inhibits TGF-β1 proliferative activity by inhibiting the Smad signaling. [42]Decorin inhibitory activity allows it to reduce fibrosis in cardiac, and renal models.[43,44] Prior research has also indicated that decorin has other roles besides interacting with TGF-β1 including regulating collagen fibrillogenesis, a process that provides structure for tissues.[45,46]In the heart, collagen is a critical protein as the extracellular matrix is mainly made up of collagen.[47] Excessive accumulation of this protein can cause changes in electrical conductions leading to arrhythmias.[48] Decorin-enriched EVs exhibited an antifibrotic response as compared to decorin-depleted EVs, providing insight into the specific molecules EVs use to produce this effect.

There are many advantages to using EVs as therapy as compared to protein due to their properties. EVs are particles that are biocompatible, unconstrained by biological barriers, and consist of a cargo with molecules derived from their parental cell.[49–51] In addition to this, EVs have a lipid bilayer which may be involved in protecting its cargo.[52] EVs are also beneficial drug delivery systems as compared to protein therapy due to their fast removal from systemic circulation by the kidneys.[53] EVs also consist of many molecules therefore, allowing for multiple pathways to be targeted. Previous studies have demonstrated that in cardiovascular diseases, EVs have the potential to decrease cell apoptosis,

reduce tissue fibrosis, and inhibit cell autophagy.[54] This study has added to the literature by highlighting decorin as a molecule within EVs with anti-fibrotic effects in atrial fibroblasts. This can also lead to the possibility of engineering EVs to enrich them further with decorin to ensure a large fibrotic effect.

Despite these findings, this study has some limitations that need to be addressed. Firstly, despite employing two assays (CCK8 and Hoechst) to measure cell proliferation, other endpoints should also be investigated. For instance, collagen deposition, and myofibroblast differentiation should be analyzed as they are altered in fibrosis.[55]These assays would have provided further insight into the effect decorin - enriched EVs have on fibrosis. It would also be beneficial to normalize EV dosing within these experiments to protein levels to ensure comparability between decorin-depleted and decorin-enriched EV samples. Moreover, concentrations of EV samples varied across the 3 donors, with a coefficient of variation of ~34% (**Figure 5**). While there was still a sufficient yield of donor-specific EVs (not pooled) for downstream assays, the donor variability may limit the generalizability of our findings. Additionally, decorin specificity in the TEM images can be improved by including isotype or no-primary antibody controls. In addition to this, the experiments in this study were conducted in vitro therefore, we can't evaluate factors that may affect the potential of decorin-enriched and decorin-depleted EVs in reducing fibrosis. An animal model would have provided insight into systemic interactions, and therapeutic efficacy.[56]Furthermore, there is an absence of decorin rescue experiments, which limits our ability to establish its causal role. This can be included in future studies.

In summary, the findings from our experiment are clinically relevant as they provide insight into EVs mechanistic pathways that contribute to anti-fibrosis. POAF is a common yet expensive complication that can cause cost patients $10,000-$20,000 in treatments, a day to two days stay in the ICU, and an additional stay of a few days at the hospital.[57,58] Fibrosis develops the atrial substrate leading to persistent

arial fibrillation.[59]Decorin -enriched EVs is a promising therapeutic for POAF as it targets fibrosis, which is one of the underlying causes of POAF.

Conclusion

Decorin-enriched EVs are a promising therapeutic to prevent POAF by reducing inflammation and fibrosis. This will be impactful as there are many cardiac patients affected by POAF, a condition associated with increases in incidence of mortality and morbidity. [60]Conventional therapies lack efficacy such as beta blockersor angiotensin-converting enzyme inhibitor therapy may lead to a recurrence of POAF.[61] However, the use of EVs enriched with decorin reduce fibrosis in vitro by decreasing cell proliferation as measured by CCK8 and Hoechst. Overall, indicating that EVs may have a potential to be more effective than conventional therapies.

Supplemental Figures

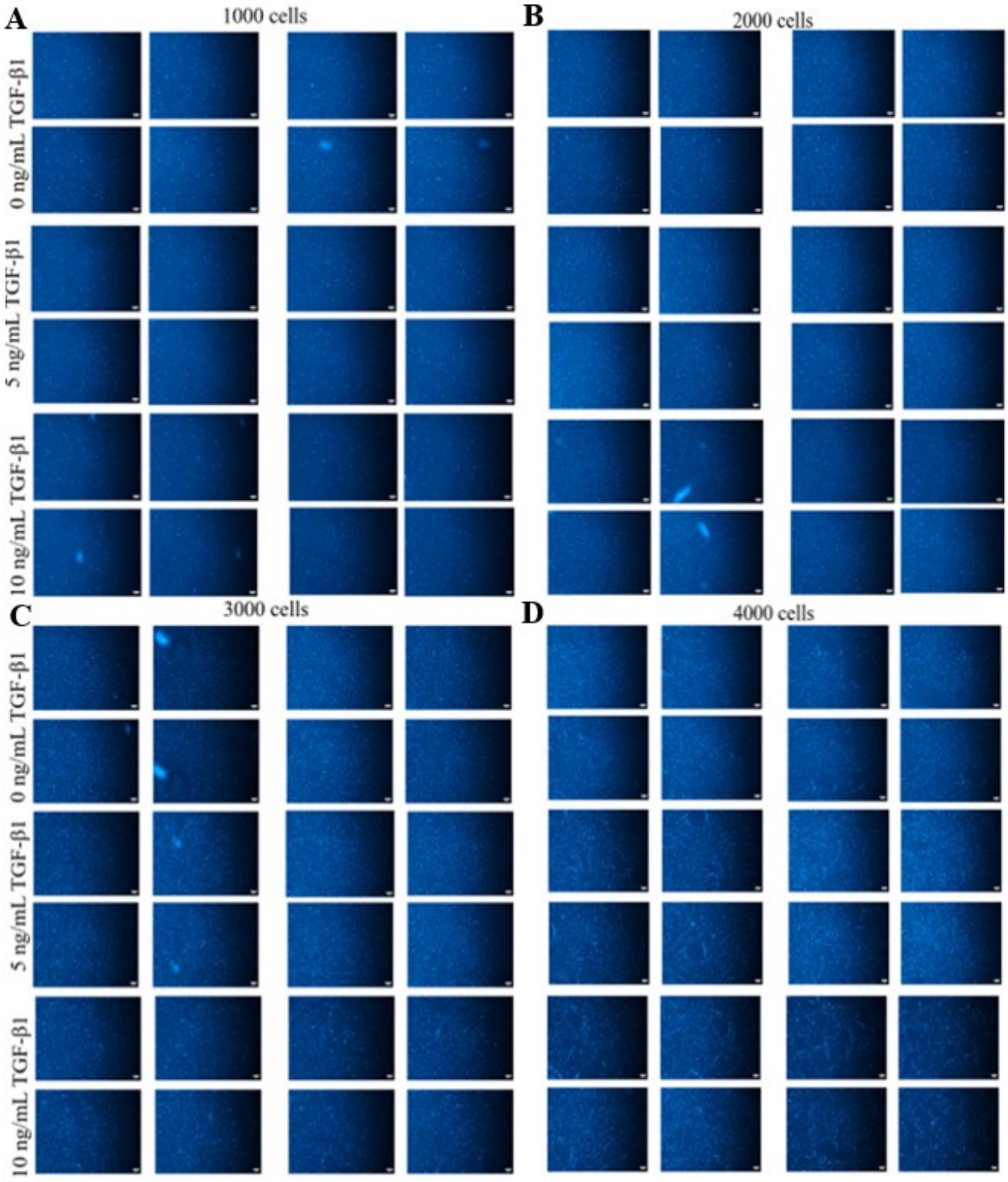

Supplementary Figure S1. Hoechst images of human atrial fibroblasts. Fibroblasts were seeded at varying densities including **(A)** 1000, **(B)** 2000, **(C)** 3000, and **(D)** 4000 cells in a 96 well plate. Cells were treated with 0 ng/mL of TGF-β1, 5 ng/mL of TGF-β1, 10 ng/mL of TGF- β1 for 48 hours.

Fluorescent microscopy was used to capture images at 5x magnification that show the Hoechst-stained nuclei of the cells in the wells. The scale bar represents 100 µm. n = 2 technical replicates per condition. These cells were from one biological sample (n = 1 biological replicate).

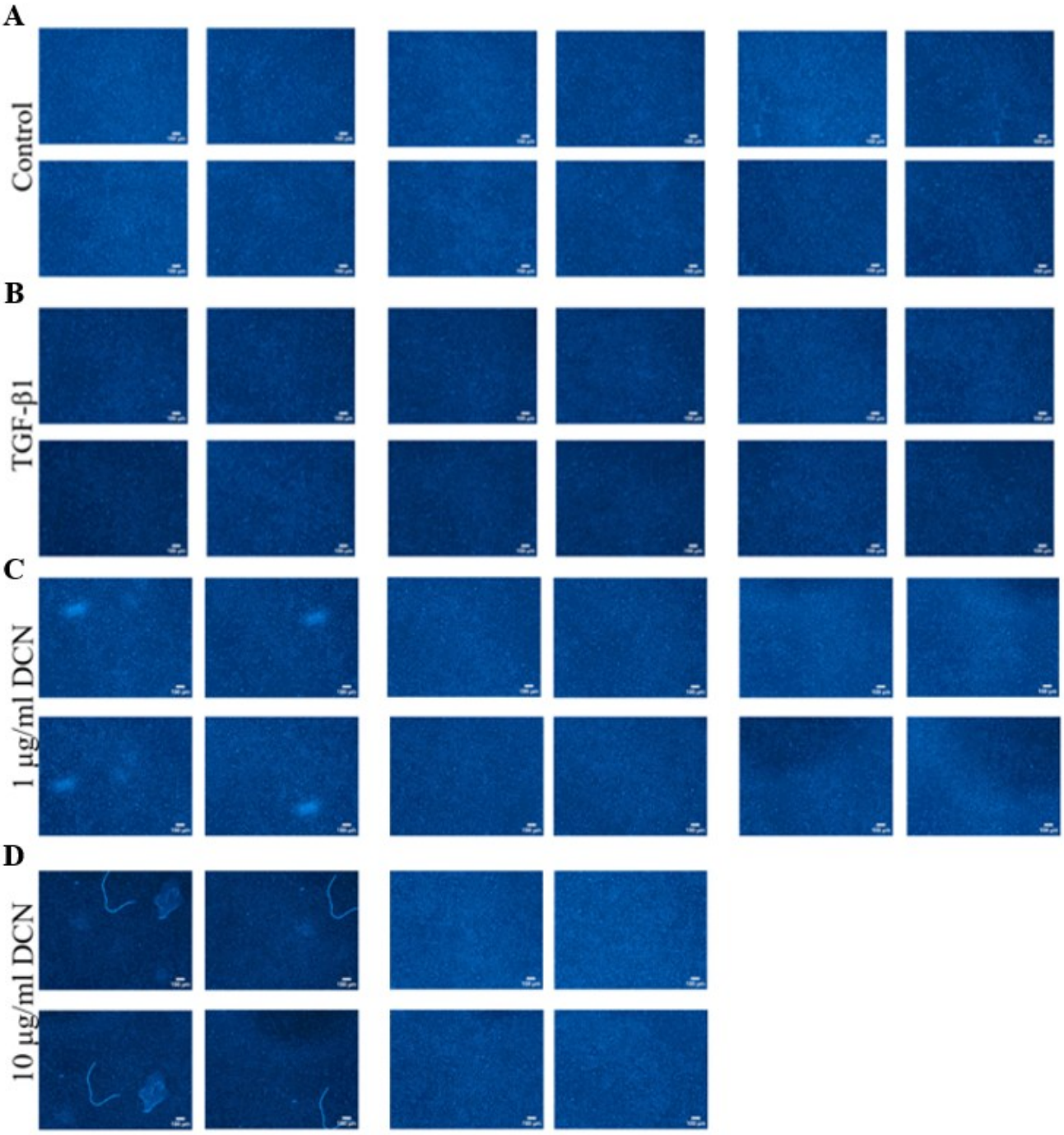

Supplementary Figure S2. Hoechst-stained images of a wells seeded human atrial fibroblasts separately treated with DCN and TGF-β1. Human atrial fibroblasts were seeded in a 96-well plate.

After 24 hours, these cells were treated separately with **(A)** media (n=3 technical replicates) **(B)** TGF-β1 (10 ng/mL) (n=3 technical replicates) **(C)** 1 µg/mL DCN (n=3 technical replicates) **(D)** 10 µg/mL DCN (n=2 technical replicates). These cells were from one biological sample (n=1 biological replicate). After 24 hours of treatment, wells were treated with Hoechst to stain nuclei. Four images of each well were captured using a fluorescent microscope at a 5x magnification. The nuclei were counted using ImageJ. The scale bar represents 100 µm.

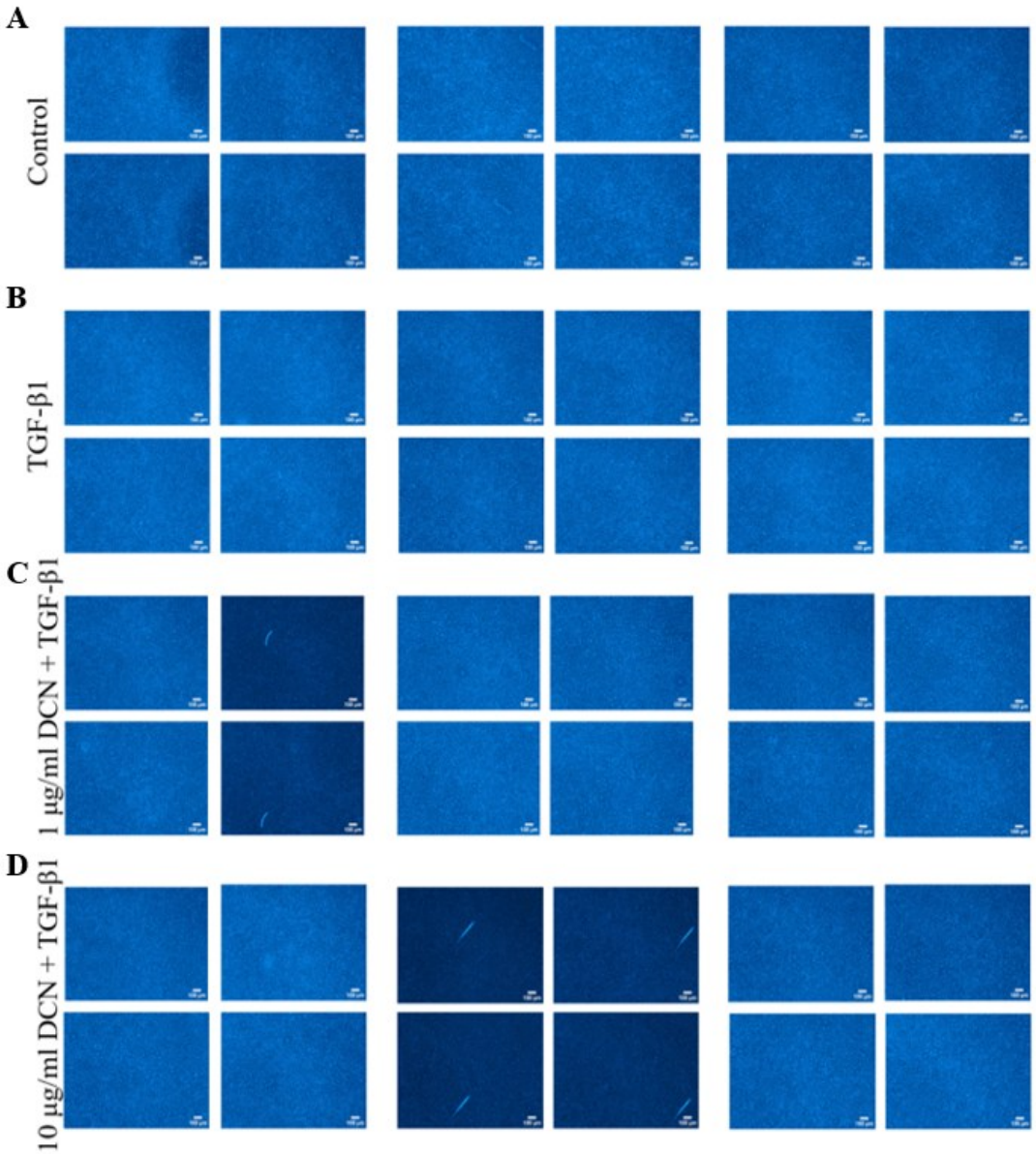

Supplementary Figure S3. Hoechst-stained images of human atrial fibroblasts co-treated with DCN (1 µg/mL or 10 µg/mL) and TGF-β1 (10 ng/mL). Cells are seeded on 96-well plates. These cells are

treated with **(A)** media **(B)** TGF-β1 **(C)** 1 µg/mL decorin + TGF-β1 **(D)** 10 µg/mL decorin + TGF-β1. 24-hour post- treatment, wells were treated with Hoechst to stain the nuclei. The wells were imaged using a fluorescent microscope and nuclei were counted using ImageJ. The scale bar represents 100 µm. n=3 technical replicates per condition. These cells were from one biological sample (n=1 biological replicate).

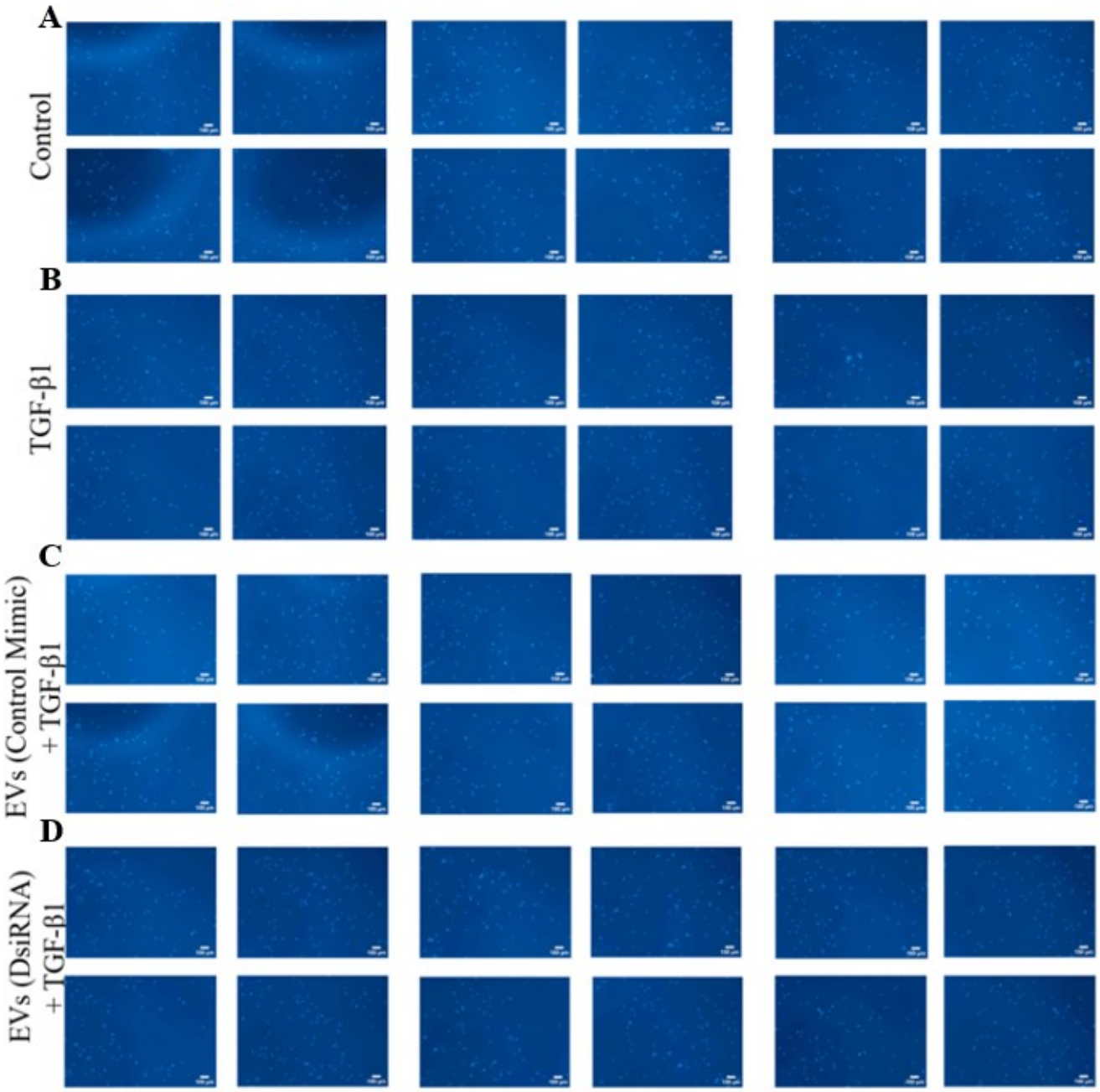

Supplementary Figure S4. Hoechst-stained images of human atrial fibroblasts co-treated with extracellular vesicles and TGF-β1. Human atrial fibroblasts were seeded in 96-well plates. These cells

were treated with **(A)** media **(B)** TGF-β1 **(C)** EVs (control mimic) with TGF-β1, and **(D)** EVs (DsiRNA) with TGF-β1. 24 hours later, Hoechst was added into each well to stain the nuclei. The nuclei were imaged using a fluorescent microscope. The scale bar represents 100 μm. n=3 technical replicates per condition. These cells were from one biological sample (n=1 biological replicate).

References

1. Gaudino M, Di Franco A, Rong LQ, Piccini J, Mack M. Postoperative atrial fibrillation: From mechanisms to treatment. *Eur Heart J.Oxford University Press*. 2023;44(12):1020-1039. doi:10.1093/eurheartj/ehad019

2. Tamargo J, Villacastín J, Caballero R, Delpón E. Drug-induced atrial fibrillation. A narrative review of a forgotten adverse effect. *Pharmacol Res*. 2024;200. doi:10.1016/j.phrs.2024.107077

3. Malektojari A, Javidfar Z, Ghazizadeh S, et al. Effectiveness of Anti-Inflammatory Agents to Prevent Atrial Fibrillation After Cardiac Surgery: A Systematic Review and Network Meta-Analysis. *CJC Open.Elsevier Inc.* Preprint posted online January 1, 2024. doi:10.1016/j.cjco.2024.10.008

4. Parent S, Amant JS, Remortel S Van, et al. Atrial Fibrosis and Inflammation in Postoperative Atrial Fibrillation: Comparative Effects of Amiodarone, Colchicine, or Exosomes. *JACC Clin Electrophysiol*. 2024;10(6):1037-1049. doi:10.1016/j.jacep.2024.02.019

5. Ziff OJ, Samra M, Howard JP, et al. Beta-blocker efficacy across different cardiovascular indications: An umbrella review and meta-analytic assessment. *BMC Med.BioMed Central Ltd.* 2020;18(1). doi:10.1186/s12916-020-01564-3

6. Welsh JA, Goberdhan DCI, O'Driscoll L, et al. Minimal information for studies of extracellular vesicles (MISEV2023): From basic to advanced approaches. *J Extracell Vesicles*. 2024;13(2). doi:10.1002/jev2.12404

7. Parent S, Vaka Ramana, Risha Yousef, et al. Prevention of atrial fibrillation after open-chest surgery with extracellular vesicle therapy. *JCI Insight*. Published online June 29, 2023.

8. Doyle LM, Wang MZ. Overview of extracellular vesicles, their origin, composition, purpose, and methods for exosome isolation and analysis. *Cells.MDPI*. 2019;8(7). doi:10.3390/cells8070727

9. Yu J, Sane S, Kim JE, et al. Biogenesis and delivery of extracellular vesicles: harnessing the power of EVs for diagnostics and therapeutics. *Front Mol Biosci*.*Frontiers Media SA*. 2023;10. doi:10.3389/fmolb.2023.1330400

10. Hosseinkhani B, Kuypers S, van den Akker NMS, Molin DGM, Michiels L. Extracellular vesicles work as a functional inflammatory mediator between vascular endothelial cells and immune cells. *Front Immunol*. 2018;9(AUG). doi:10.3389/fimmu.2018.01789

11. Černe K, Kelhar N, Resnik N, et al. Characteristics of Extracellular Vesicles from a High-Grade Serous Ovarian Cancer Cell Line Derived from a Platinum-Resistant Patient as a Potential Tool for Aiding the Prediction of Responses to Chemotherapy. *Pharmaceuticals*. 2023;16(6). doi:10.3390/ph16060907

12. Wang MC, Gong GY, Wang CL, et al. Methods for Collection of Extracellular Vesicles and Their Content RNA as Liquid Biopsy for Lung Cancer Detection: Application of Differential Centrifugation and Annexin A5 Coated Beads. *Curr Issues Mol Biol*. 2022;44(5):2374-2386. doi:10.3390/cimb44050162

13. Parent S, Vaka R, Amant JS, et al. Inactivation of the NLRP3 inflammasome mediates exosome based prevention of atrial fibrillation. *Theranostics*. 2024;14(2):608-621. doi:10.7150/thno.89520

14. Gauthier BR, Cobo-Vuilleumier N, López-Noriega L. Roles of extracellular vesicles associated non-coding RNAs in Diabetes Mellitus. *Front Endocrinol (Lausanne)*.*Frontiers Media S.A.* 2022;13. doi:10.3389/fendo.2022.1057407

15. Ginini L, Billan S, Fridman E, Gil Z. Insight into Extracellular Vesicle-Cell Communication: From Cell Recognition to Intracellular Fate. *Cells*.*MDPI*. 2022;11(9). doi:10.3390/cells11091375

16. Zhang W, Ge Y, Cheng Q, et al. *Decorin Is a Pivotal Effector in the Extracellular Matrix and*

Tumour Microenvironment THE STRUCTURE AND INACTIVATION OF DCN. Vol 9.; 2018. www.impactjournals.com/oncotarget

17. Baghy K, Szakadáti H, Kovalszky I. Decorin the antifibrotic proteoglycan and its progression in therapy. *Am J Physiol Cell Physiol.American Physiological Society*. 2025;328(6):C1853-C1865. doi:10.1152/ajpcell.01075.2024

18. Plichta J, Panek M. Role of the TGF-β cytokine and its gene polymorphisms in asthma etiopathogenesis. *Frontiers in Allergy.Frontiers Media SA*. 2025;6. doi:10.3389/falgy.2025.1529071

19. Nüchel J, Ghatak S, Zuk A V., et al. TGFB1 is secreted through an unconventional pathway dependent on the autophagic machinery and cytoskeletal regulators. *Autophagy*. 2018;14(3):465-486. doi:10.1080/15548627.2017.1422850

20. Deng Z, Fan T, Xiao C, et al. TGF-β signaling in health, disease, and therapeutics. *Signal Transduct Target Ther.Springer Nature*. 2024;9(1). doi:10.1038/s41392-024-01764-w

21. McIntyre WF. Post-operative atrial fibrillation after cardiac surgery: Challenges throughout the patient journey. *Front Cardiovasc Med.Frontiers Media S.A.* 2023;10. doi:10.3389/fcvm.2023.1156626

22. Lotter K, Yadav S, Saxena P, Vangaveti V, John B. Predictors of atrial fibrillation post coronary artery bypass graft surgery: new scoring system. *Open Heart*. 2023;10(1). doi:10.1136/openhrt-2023-002284

23. Meenashi Sundaram D, Vasavada AM, Ravindra C, Rengan V, Meenashi Sundaram P. The Management of Postoperative Atrial Fibrillation (POAF): A Systematic Review. *Cureus*. Published online August 3, 2023. doi:10.7759/cureus.42880

24. Yang J, Zou X, Jose PA, Zeng C. Extracellular vesicles: Potential impact on cardiovascular diseases. In: *Advances in Clinical Chemistry*. Vol 105. Academic Press Inc.; 2021:49-100. doi:10.1016/bs.acc.2021.02.002

25. Moore-Morris T, Cattaneo P, Puceat M, Evans SM. Origins of cardiac fibroblasts. *J Mol Cell Cardiol.Academic Press*. 2016;91:1-5. doi:10.1016/j.yjmcc.2015.12.031

26. Xu Q, Norman JT, Shrivastav S, Lucio-Cazana J, Kopp JB. Innovative Methodology In vitro models of TGF-induced fibrosis suitable for high-throughput screening of antifibrotic agents. *Am J Physiol Renal Physiol*. 2007;293:631-640. doi:10.1152/ajprenal.00379.2006.-Progressive

27. Spicer S, Hasheminia A, Kandi S, Abu-Omar Y, Fernández ÁL, El-Diasty M. Cardiac and pericardial inflammatory changes and post-cardiac surgery atrial fibrillation. *Cytokine Growth Factor Rev.Elsevier Ltd*. Preprint posted online 2025. doi:10.1016/j.cytogfr.2025.07.006

28. Fan J, Schiemer T, Vaska A, Jahed V, Klavins K. Cell via Cell Viability Assay Changes Cellular Metabolic Characteristics by Intervening with Glycolysis and Pentose Phosphate Pathway. *Chem Res Toxicol*. 2024;37(2):208-211. doi:10.1021/acs.chemrestox.3c00339

29. Fan J, Schiemer T, Vaska A, Jahed V, Klavins K. Cell via Cell Viability Assay Changes Cellular Metabolic Characteristics by Intervening with Glycolysis and Pentose Phosphate Pathway. *Chem Res Toxicol*. 2024;37(2):208-211. doi:10.1021/acs.chemrestox.3c00339

30. Șorodoc V, Indrei L, Dobroghii C, et al. Amiodarone Therapy: Updated Practical Insights. *J Clin Med.Multidisciplinary Digital Publishing Institute (MDPI)*. 2024;13(20). doi:10.3390/jcm13206094

31. A. Lopes L, K. Agrawal D. Post-Operative Atrial Fibrillation: Current Treatments and Etiologies for a Persistent Surgical Complication. *J Surg Res (Houst)*. 2022;05(01). doi:10.26502/jsr.10020209

32. Liu S, Wu X, Chandra S, et al. Extracellular vesicles: Emerging tools as therapeutic agent carriers. *Acta Pharm Sin B.Chinese Academy of Medical Sciences*. 2022;12(10):3822-3842. doi:10.1016/j.apsb.2022.05.002

33. Liu C, Bayado N, He D, et al. Therapeutic Applications of Extracellular Vesicles for Myocardial Repair. *Front Cardiovasc Med.Frontiers Media SA*. 2021;8. doi:10.3389/fcvm.2021.758050

34. Parent S, Vaka R, Amant JS, et al. Inactivation of the NLRP3 inflammasome mediates exosomebased prevention of atrial fibrillation. *Theranostics*. 2024;14(2):608-621. doi:10.7150/thno.89520

35. Tjahjono NS, Subramanian D, Shihabeddin TZ, et al. Effect of Decorin and Aligned Collagen Fibril Topography on TGF-β1 Activation of Corneal Keratocytes. *Bioengineering*. 2025;12(3). doi:10.3390/bioengineering12030259

36. Wang P, Liu X, Xu P, Lu J, Wang R, Mu W. Decorin reduces hypertrophic scarring through inhibition of the TGF-β1/Smad signaling pathway in a rat osteomyelitis model. *Exp Ther Med*. 2016;12(4):2102-2108. doi:10.3892/etm.2016.3591

37. Wang L, Ko CY, Meyers EE, Pedroja BS, Pelaez N, Bernstein AM. *Concentration-Dependent Effects of Transforming Growth Factor B1 on Corneal Wound Healing*.; 2011. http://www.molvis.org/molvis/v17/a308

38. Chen G, Khalil N. TGF-β1 increases proliferation of airway smooth muscle cells by phosphorylation of map kinases. *Respir Res*. 2006;7. doi:10.1186/1465-9921-7-2

39. Turagam MK, Mirza M, Werner PH, et al. Circulating biomarkers predictive of postoperative atrial fibrillation. *Cardiol Rev.Lippincott Williams and Wilkins*. 2016;24(2):76-87. doi:10.1097/CRD.0000000000000059

40. Zhou X, Franklin RA, Adler M, et al. Microenvironmental sensing by fibroblasts controls macrophage population size. Published online 2022. doi:10.1073/pnas

41. Ligasová A, Koberna K. Dna dyes—highly sensitive reporters of cell quantification: Comparison with other cell quantification methods. *Molecules*.*MDPI*. 2021;26(18). doi:10.3390/molecules26185515

42. Cui J, Zhang S, Acharya K, et al. Decorin attenuates hypertrophic scar fibrosis via TGFβ/Smad signalling. *Exp Dermatol*. 2024;33(7). doi:10.1111/exd.15133

43. Jiang N, Zhang Q, Chau MK, et al. Anti-fibrotic effect of decorin in peritoneal dialysis and PDassociated peritonitis. *EBioMedicine*. 2020;52. doi:10.1016/j.ebiom.2020.102661

44. Mohindra P, Zhong JX, Fang Q, et al. Local decorin delivery via hyaluronic acid microrods improves cardiac performance, ventricular remodeling after myocardial infarction. *NPJ Regen Med*. 2023;8(1). doi:10.1038/s41536-023-00336-w

45. Kular JK, Basu S, Sharma RI. The extracellular matrix: Structure, composition, age-related differences, tools for analysis and applications for tissue engineering. *J Tissue Eng*.*SAGE Publications Ltd*. 2014;5. doi:10.1177/2041731414557112

46. Gubbiotti MA, Vallet SD, Ricard-Blum S, Iozzo R V. Decorin interacting network: A comprehensive analysis of decorin-binding partners and their versatile functions. *Matrix Biology*.*Elsevier B.V.* 2016;55:7-21. doi:10.1016/j.matbio.2016.09.009

47. Kallergis EM, Goudis CA, Kanoupakis EM, et al. Sinus rhythm restoration affects collagen turnover in patients with persistent atrial fibrillation. *Europace*. 2014;16(12):1726-1730. doi:10.1093/europace/eut401

48. Saheera S, Krishnamurthy P. Cardiovascular Changes Associated with Hypertensive Heart Disease and Aging. *Cell Transplant*.*SAGE Publications Ltd*. 2020;29. doi:10.1177/0963689720920830

49. Bahmani L, Ullah M. Different Sourced Extracellular Vesicles and Their Potential Applications in Clinical Treatments. *Cells.MDPI*. 2022;11(13). doi:10.3390/cells11131989

50. Zeng B, Li Y, Xia J, et al. Micro Trojan horses: Engineering extracellular vesicles crossing biological barriers for drug delivery. *Bioeng Transl Med.John Wiley and Sons Inc*. 2024;9(2). doi:10.1002/btm2.10623

51. Cheng W, Xu C, Su Y, et al. Engineered Extracellular Vesicles: A potential treatment for regeneration. *iScience.Elsevier Inc.* 2023;26(11). doi:10.1016/j.isci.2023.108282

52. Ghadami S, Dellinger K. The lipid composition of extracellular vesicles: applications in diagnostics and therapeutic delivery. *Front Mol Biosci.Frontiers Media SA*. 2023;10. doi:10.3389/fmolb.2023.1198044

53. Haddadzadegan S, Dorkoosh F, Bernkop-Schnürch A. Oral delivery of therapeutic peptides and proteins: Technology landscape of lipid-based nanocarriers. *Adv Drug Deliv Rev.Elsevier B.V.* 2022;182. doi:10.1016/j.addr.2021.114097

54. Fu S, Zhang Y, Li Y, Luo L, Zhao Y, Yao Y. Extracellular vesicles in cardiovascular diseases. *Cell Death Discov.Springer Nature*. 2020;6(1). doi:10.1038/s41420-020-00305-y

55. Frangogiannis NG. Cardiac fibrosis: Cell biological mechanisms, molecular pathways and therapeutic opportunities. *Mol Aspects Med.Elsevier Ltd*. 2019;65:70-99. doi:10.1016/j.mam.2018.07.001

56. Mukherjee P, Roy S, Ghosh D, Nandi SK. Role of animal models in biomedical research: a review. *Lab Anim Res.BioMed Central Ltd*. 2022;38(1). doi:10.1186/s42826-022-00128-1

57. Greenberg JW, Lancaster TS, Schuessler RB, Melby SJ. Postoperative atrial fibrillation following cardiac surgery: A persistent complication. *European Journal of Cardio-thoracic Surgery.European Association for Cardio-Thoracic Surgery*. 2017;52(4):665-672.

doi:10.1093/ejcts/ezx039

58. Echahidi N, Pibarot P, O'Hara G, Mathieu P. Mechanisms, Prevention, and Treatment of Atrial Fibrillation After Cardiac Surgery. *J Am Coll Cardiol*. 2008;51(8):793-801. doi:10.1016/j.jacc.2007.10.043

59. Al-Kaisey AM, Parameswaran R, Kalman JM. Atrial fibrillation structural substrates: Aetiology, identification and implications. *Arrhythm Electrophysiol Rev*. 2020;9(3). doi:10.15420/AER.2020.19

60. Lapar DJ, Speir AM, Crosby IK, et al. Postoperative atrial fibrillation significantly increases mortality, hospital readmission, and hospital costs. *Annals of Thoracic Surgery*. 2014;98(2):527-533. doi:10.1016/j.athoracsur.2014.03.039

61. Shah S, Chahil V, Battisha A, Haq S, Kalra DK. Postoperative Atrial Fibrillation: A Review. *Biomedicines*.*Multidisciplinary Digital Publishing Institute (MDPI)*. 2024;12(9). doi:10.3390/biomedicines12091968